Polysaccharide breakdown products drive degradation-dispersal cycles of foraging bacteria through changes in metabolism and motility

Astrid K.M. Stubbusch[1,2,3], Johannes M. Keegstra[4], Julia Schwartzman[5,6], Sammy Pontrelli[7], Estelle E. Clerc[4], Samuel Charlton[4], Roman Stocker[4], Cara Magnabosco[3], Olga T. Schubert[1,2], Martin Ackermann[1,2,8], Glen G. D'Souza[1,2]

[1]Institute of Biogeochemistry and Pollutant Dynamics, Department of Environmental Systems Science, ETH Zurich, Zurich, Switzerland
[2]Department of Environmental Microbiology, Eawag: Swiss Federal Institute of Aquatic Science and Technology, Dübendorf, Switzerland
[3]Geological Institute, Department of Earth Sciences, ETH Zurich, Zurich, Switzerland
[4]Institute of Environmental Engineering, Department of Civil, Environmental and Geomatic Engineering, ETH Zurich, Zurich, Switzerland
[5]Department of Civil and Environmental Engineering, MIT, Cambridge, MA, USA
[6]Department of Biology, University of Southern California, Los Angeles, USA
[7]Institute of Molecular Systems Biology, Department of Biology, ETH Zurich, Zurich, Switzerland
[8]Laboratory of Microbial Systems Ecology, School of Architecture, Civil and Environmental Engineering (ENAC), École Polytechnique Fédéral de Lausanne (EPFL), Lausanne, Switzerland

ORCID
AS: 0000-0003-4767-2712
JK: 0000-0002-8877-4881
JS: 0000-0003-4563-4835
SP: 0000-0001-6265-8842
EC: 0009-0003-6046-2856
SC: 0000-0002-0091-5134
RS: 0000-0002-3199-0508
CM: 0000-0001-6871-7188
OS: 0000-0002-2613-0714
MA: 0000-0003-0087-4819
GD: 0000-0002-9123-101X

Corresponding authors: Glen G D'Souza and Astrid KM Stubbusch
Address: Eawag, Ueberlandstrasse 133, 8600 Dübendorf, Switzerland
Email: glengeralddsouza@gmail.com, astubbusch@icloud.com
Phone: +41-58-765-5495

Keywords: cooperative polysaccharide degradation, colony formation, cell dispersal, glycan, alginate, exoenzymes, alginate lyases, *Vibrio cyclitrophicus* ZF270

Abstract

Most of Earth's biomass is composed of polysaccharides. During biomass decomposition, polysaccharides are degraded by heterotrophic bacteria as a nutrient and energy source and are thereby partly remineralized into CO_2. As polysaccharides are heterogeneously distributed in nature, following the colonization and degradation of a polysaccharide hotspot the cells need to reach new polysaccharide hotspots. Even though many studies indicate that these degradation-dispersal cycles contribute to the carbon flow in marine systems, we know little about how cells alternate between polysaccharide degradation and motility, and which environmental factors trigger this behavioral switch. Here, we studied the growth of the marine bacterium *Vibrio cyclitrophicus* ZF270 on the abundant marine polysaccharide alginate, both in its soluble polymeric form as well as on its breakdown products. We used microfluidics coupled to time-lapse microscopy to analyze motility and growth of individual cells, and RNA sequencing to study associated changes in gene expression. We found that single cells grow at reduced rate on alginate until they form large groups that cooperatively break down the polymer. Exposing cell groups to digested alginate accelerates cell growth and changes the expression of genes involved in alginate degradation and catabolism, central metabolism, ribosomal biosynthesis, and transport. However, exposure to digested alginate also triggers cells to become motile and disperse from cell groups, proportionally increasing with the group size before the nutrient switch, and this is accompanied by high expression of genes involved in flagellar assembly, chemotaxis, and quorum sensing. The motile cells chemotax toward polymeric but not digested alginate, likely enabling them to find new polysaccharide hotspots. Overall, our findings reveal cellular mechanisms that might also underlie bacterial degradation-dispersal cycles, which influence the remineralization of biomass in marine environments.

Importance

Polysaccharides, also known as glycans, are the most abundant form of biomass on Earth and understanding how they are degraded by microorganisms is essential for our understanding of the global carbon cycle and the storage and release of CO_2 by natural systems. Although group formation is a

common strategy used by bacterial cells to degrade ubiquitous polymeric growth substrates in nature, where nutrient hotspots are heterogeneously distributed, little is known about how cells prepare for dispersal from an exhausted nutrient source and re-initiate degradation of new nutrient patches. By quantifying growth, motility and chemotaxis of individual cells and comparing gene expression changes when populations were exposed to either polysaccharides or their degradation products in the form of digested polysaccharides, we show that bacterial cells alter their behavior when they experience a shift from polymeric to digested polysaccharides: After cells form groups during growth on polymers, the exposure to degradation products triggered cells to become motile, enabling dispersal from sessile cell groups. The chemotactic attraction of motile cells to polymeric alginate likely allows cells to move towards new polysaccharide hotspots. Our study sheds light on the cellular processes that drive bacterial growth and behavior during carbon remineralization, an important process resulting in CO_2 release from natural systems.

Introduction

Polysaccharides represent the largest fraction of biomass on Earth[1,2] and are constantly degraded and remineralized by microorganisms. Polysaccharides, also known as glycans, are long chains of monosaccharide units produced by cells for structural support (e.g., cellulose, chitin, and alginate) or energy storage (e.g., starch or glycogen)[1]. Heterotrophic microbes obtain nutrients and energy from the polysaccharide breakdown products. They often use exoenzymes, either secreted or anchored in the cell membrane[2,3], to cleave these large polymers into smaller units that can be taken up by cells. The formation of dense cell groups is observed during growth on polysaccharides by diverse bacteria, including the soil- and gut-dwelling *Bacillus subtilis*[3], the oligotrophic fresh-water *Caulobacter crescentus*[4], and several representatives of the copiotrophic[5,6] marine *Vibrio spp.*[7,8]. It has been suggested that "cooperative" growth[3], where dense cell groups reduce diffusional loss of valuable degradation products and secreted exoenzymes, represents a general principle in polysaccharide

degradation[4,8]. Yet, how bacteria subsequently disperse from exhausted polysaccharide sources and navigate towards new polysaccharide hotspots remains poorly understood.

To study the cellular mechanisms that govern the switch between polysaccharide degradation and dispersal toward new polysaccharide hotspots, we worked with the ubiquitous marine Gammaproteobacterium *Vibrio cyclitrophicus* ZF270, a degrader of the prevalent marine polysaccharide alginate[6,9]. Alginate is a linear polysaccharide that is produced by brown algae as a cell wall component, as well as by certain bacteria. It can be cleaved into oligomers by endo-acting alginate lyases or into monomers by exo-acting alginate lyases (alginate lyases reviewed here[10]), namely β-D-mannuronic acid and α-L-guluronic acid[11]. *V. cyclitrophicus* ZF270 is found predominantly in the large-particle fractions of coastal water[12], can attach and form biofilms on the surfaces of multiple polysaccharides including alginate[13], and was shown to secrete alginate lyases during alginate degradation[8]. In this study, we used microfluidics coupled to automated time-lapse imaging to quantify the growth dynamics, group formation, and motility of *V. cyclitrophicus* ZF270 at the single-cell level under constant supply of either polymeric alginate or alginate degradation product in the form of digested alginate, as well as upon a transition from alginate to digested alginate. Furthermore, we used RNA-sequencing to compare the gene expression of *V. cyclitrophicus* ZF270 grown on alginate and digested alginate. We found striking responses to the form of alginate in growth rate, group formation, motility and chemotaxis, as well as in the expression of corresponding genes. Overall, our work provides insights into the metabolic and cellular regulation that allows cells to forage in heterogeneous nutrient-scapes through degradation-dispersal cycles.

Results

Extracellular break down of alginate delays population growth

To probe the phenotypic and metabolic regulation of bacterial cells during the progressive degradation of a polysaccharide source, we developed an experimental system consisting of the marine bacterium *V. cyclitrophicus* ZF270 growing on alginate, a highly abundant polysaccharide in the ocean. To mimic the local nutrient environment during the colonization of a new polysaccharide source, we used 0.1%

weight per volume (w/v) algae-derived alginate in its soluble form (in the following also simply referred to as "alginate"). Since commercially available alginate breakdown products of specific sizes are limited and expensive, with only one monomeric component available at a considerable cost, we simulate an advanced stage of polysaccharide degradation by supplying cells with digested alginate (0.1% (w/v)). This digested alginate is prepared by treating alginate with a readily available endo-acting alginate lyase (see Materials and Methods). This mimics an environment where degradation products like monomers and oligomers become abundant through the action of extracellular alginate lyases. The commercially available alginate lyase has been shown to produce alginate oligomers of progressively smaller size over extended digestion periods[14]. We used Liquid Chromatography-Mass Spectrometry (LC-MS) to analyze the composition of the digested alginate, which had been subject to 48 hours of digestion. We found that digested alginate contained more monosaccharides than untreated alginate, which contained more alginate molecules of higher molecular weight (Fig. S1).

Using this system, we first set out to investigate the growth dynamics of *V. cyclitrophicus* ZF270 in well-mixed batch cultures containing either alginate or digested alginate as a sole carbon source (Fig. S2A). Measurements of optical density showed that the onset of growth on alginate was delayed by about 7.5 hours compared to growth on digested alginate (Fig. S2B, D and E). This is consistent with previous observations that in well-mixed environments the lag time of bacteria growing on alginate can be reduced by the external supplementation of alginate lyases[8]. We also observed that the optical density at stationary phase was higher when cells were grown on alginate (Fig. S2B and C). However, colony counts did not show a significant difference in cell numbers (Fig. S3), suggesting that the increased optical density may stem from aggregation of cells in the alginate medium, as observed for other *Vibrio* species[7]. Overall, these findings indicate that growth on polysaccharides such as alginate in well-mixed cultures is initially limited by the extracellular breakdown of the polysaccharide, though similar cell numbers were reached eventually.

Large cell groups form on alginate but not on digested alginate

150 To better understand how cells react to the changing degree of depolymerization of a polysaccharide
151 source during degradation, we investigated the growth of *V. cyclitrophicus* ZF270 at the level of single
152 cells on alginate and digested alginate. For this purpose, we grew the cells in microfluidic growth
153 chambers, as depicted in Figure 1A and described in detail by Dal Co et al.[15]. In brief, the microfluidic
154 chips are made of an inert polymer (polydimethylsiloxane) bound to a glass coverslip. The PDMS layer
155 contains flow channels through which the culture medium is pumped continuously. Each channel is
156 connected to several growth chambers that are laterally positioned. The dimensions of these growth
157 chambers (height: 0.85 µm, length: 60 µm, width: 90-120 µm) allow cells to freely move and grow as
158 monolayers. The culture medium, containing either alginate or digested alginate in their soluble form,
159 is constantly pumped through the flow channel and enters the growth chambers primarily through
160 diffusion[15,16,4,17,8]. Therefore, the number of cells and their positioning within microfluidic chambers is
161 determined by the cellular growth rate as well as by cell movement[4]. This setup combined with time-
162 lapse microscopy allowed us to follow the development of cell communities over time. We found that
163 over 24 hours dense groups of more than 1000 cells formed on alginate, filling the entire microfluidic
164 chamber (Fig. 1B). In contrast, cells supplied with digested alginate grew in smaller groups that never
165 exceeded 100 cells per chamber (Fig. 1C and D). Reconstructed cell lineages revealed that the large cell
166 groups on alginate formed because cells often did not disperse after division and thereby formed dense
167 cell groups originating from a single cell lineage (Fig. 1B). The lower cell density on digested alginate
168 could be caused by slower growth or by more cells leaving the chambers. As the maximum growth rate
169 both in bulk and on single cell level is similar in alginate and digested alginate (Fig. S2E and F), it is
170 more likely that the lower cell density in digested alginate is caused by cell dispersal. To test the role
171 of increased viscosity of polymeric alginate in causing the increased aggregation of cells, we measured
172 the viscosity of 0.1% (w/v) alginate or digested alginate dissolved in TR media. For alginate, the
173 viscosity was 1.03±0.01 mPa·s (mean and standard deviation of three technical replicates) whereas the
174 viscosity of digested alginate in TR media was found to be 0.74±0.01 mPa·s. Both these values are
175 relatively close to the viscosity of water at this temperature (0.89 mPa·s[18]) and, while they may affect
176 swimming behavior[19], they are insufficient to physically restrain cell movement[20]. Overall, our
177 observations suggest that cells can modulate their propensity to form groups depending on the state of

178 polysaccharide degradation in their local environment. Similar observations were made with a different
179 model system (*Caulobacter crescentus* growing on the polysaccharide xylan)[16], indicating that group
180 formation on polymeric nutrient sources may be a general mechanism of bacteria that degrade
181 polysaccharides extracellularly.
182

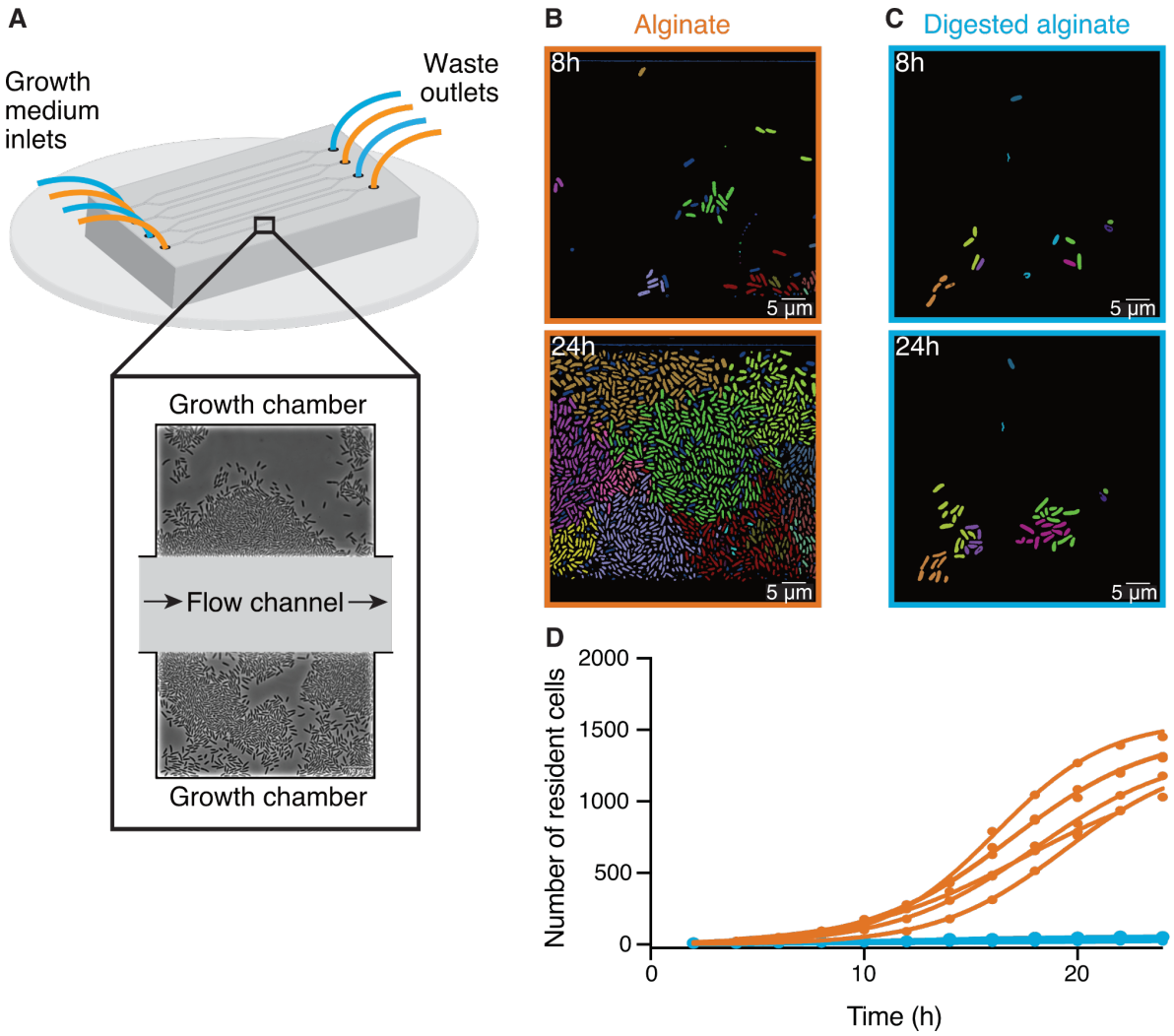

183
184 **Figure 1. Large cell groups form on alginate but not on digested alginate.** (A) Schematic representation of the
185 setup of the microfluidic experiments. (B and C) Representative images at different time points of *V.*
186 *cyclitrophicus* ZF270 cells growing in microfluidic chambers, described in detail by Dal Co et al.[15], with (B)
187 alginate medium or (C) digested alginate medium, both in their soluble form (not visible). Cells are false-colored
188 according to their lineage identities based on cell segmentation and tracking over 24 hours. Cells without identified
189 progenitors are colored in dark blue. See Supplemental Videos S1 (alginate) and S2 (digested alginate) for time-
190 lapse videos. (D) Cell numbers within microfluidic chambers supplied with alginate (orange) are substantially

191 higher than cell numbers within microfluidic chambers supplied with digested alginate (blue) (Logistic growth
192 regression for alginate: R^2 = 0.99, maximal number of cells = 1217-1564, k = 0.24-0.38 h^{-1}; for digested alginate:
193 R^2 = 0.86-0.97, maximal number of cells = 47-100, k = 0.07-0.4 h^{-1}). Circles indicate the number of cells present
194 at a given time point in each chamber ($n_{chambers}$ = 7). Data for chambers with alginate originate from D'Souza et
195 al.[8]. Lines are fits of a logistic growth regression line for each condition.
196

197 **Transition from alginate to digested alginate triggers density-dependent dispersal of cells**

198 To investigate the transition from the large cell groups formed on alginate to the small groups formed
199 on digested alginate, we subjected *V. cyclitrophicus* ZF270 cells grown on alginate to a switch to
200 digested alginate (Fig. 2A). Following the limited cell motility on alginate, this switch led to a rapid
201 decrease in cell density within the growth chambers (Fig. 2B), presumably caused by cell dispersal. As
202 we previously reported for other *Vibrionaceae* isolates, the growth rate of the cells on alginate was
203 dependent on the local cell density: Initially the growth rate increased with cell density but then
204 decreased at high cell densities, indicating that cell groups can benefit from the sharing of breakdown
205 products generated by each other's exoenzymes, but also increasingly compete for nutrients[8]. This led
206 us to investigate whether cells in larger groups, potentially experiencing stronger nutrient competition,
207 might have a higher propensity to disperse after a switch to digested alginate than cells in smaller
208 groups. We indeed found that the nutrient switch caused a few or no cells to disperse from small cell
209 groups (Fig. 2B), whereas a large fraction of cells from large cell groups dispersed (Fig. 2C). In fact,
210 the fraction of cells that dispersed upon imposition of the nutrient switch showed a strong positive
211 relationship with the number of cells present, meaning that cells in chambers with many cells were more
212 likely to disperse than cells in chambers with fewer cells (Fig. 2C). Thus, during the transition from
213 polysaccharides to degradation products, we found that the dispersal rate of cells depends on the size of
214 the cell groups, likely through increased motility of cells in large groups.
215

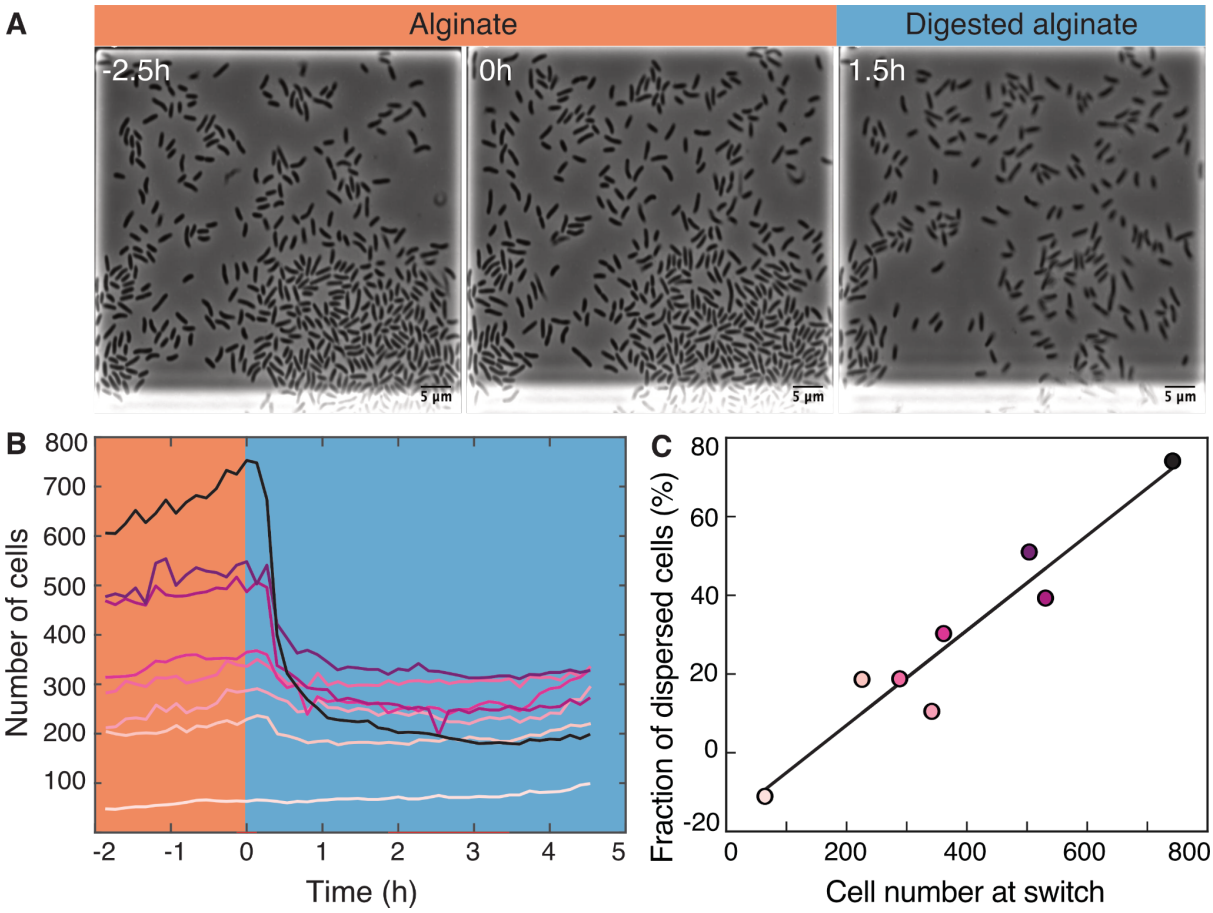

Figure 2. Transition from alginate to digested alginate triggers density-dependent dispersal of cells. (A) Representative time-lapse images of *V. cyclitrophicus* ZF270 cells (phase contrast microscopy) in microfluidic growth chambers that were initially exposed to alginate and then switched to digested alginate. (B) Number of cells in different chambers over time, each chamber indicated by a unique color (n = 8). The carbon source is indicated by the colored background (orange: alginate; blue: digested alginate). See Supplemental Video 3 for a time-lapse video. (C) Positive relationship between the number of cells in the microfluidic growth chamber at the time of the switch and the fraction of cells that disperse after the switch. Each circle represents one growth chamber with colors corresponding to (B), and the line depicts a linear regression fit (R^2 = 0.92, slope = 0.12).

Cells growing on digested alginate are more motile and polymeric alginate acts as chemoattractant

To investigate whether increased cell motility of *V. cyclitrophicus* ZF270 underlies the dispersal of cells observed after a shift to digested alginate, as also previously observed for *C. crescentus* cells on the monosaccharide xylose[4,16], we quantified the motility of single cells supplied with either alginate or

231 digested alginate. We found that the single-cell swimming speed as well as the swimming distance were
232 significantly larger for cells supplied with digested alginate compared to cells supplied with alginate,
233 and that a larger fraction of cells was motile (Fig. 3). This confirmed increased motility as a cellular
234 response to the exposure to degradation products in the form of digested alginate. Overall, these findings
235 suggest that once the breakdown of a polysaccharide source makes breakdown products available in the
236 local environment, a fraction of cells becomes motile and disperses.
237
238 To understand whether alginate polymers or alginate breakdown products act as chemoattractants on
239 motile cells, we measured the chemotactic strength towards alginate and digested alginate using the In
240 Situ Chemotaxis Assay (ISCA)[21,22]. Interestingly, we found *V. cyclitrophicus* ZF270 to significantly
241 chemotax toward alginate (chemotactic index $I_c > 1$) but not significantly toward digested alginate (Fig.
242 3F). This suggested that the increase in motility is accompanied by chemotaxis toward alginate
243 polymers.
244

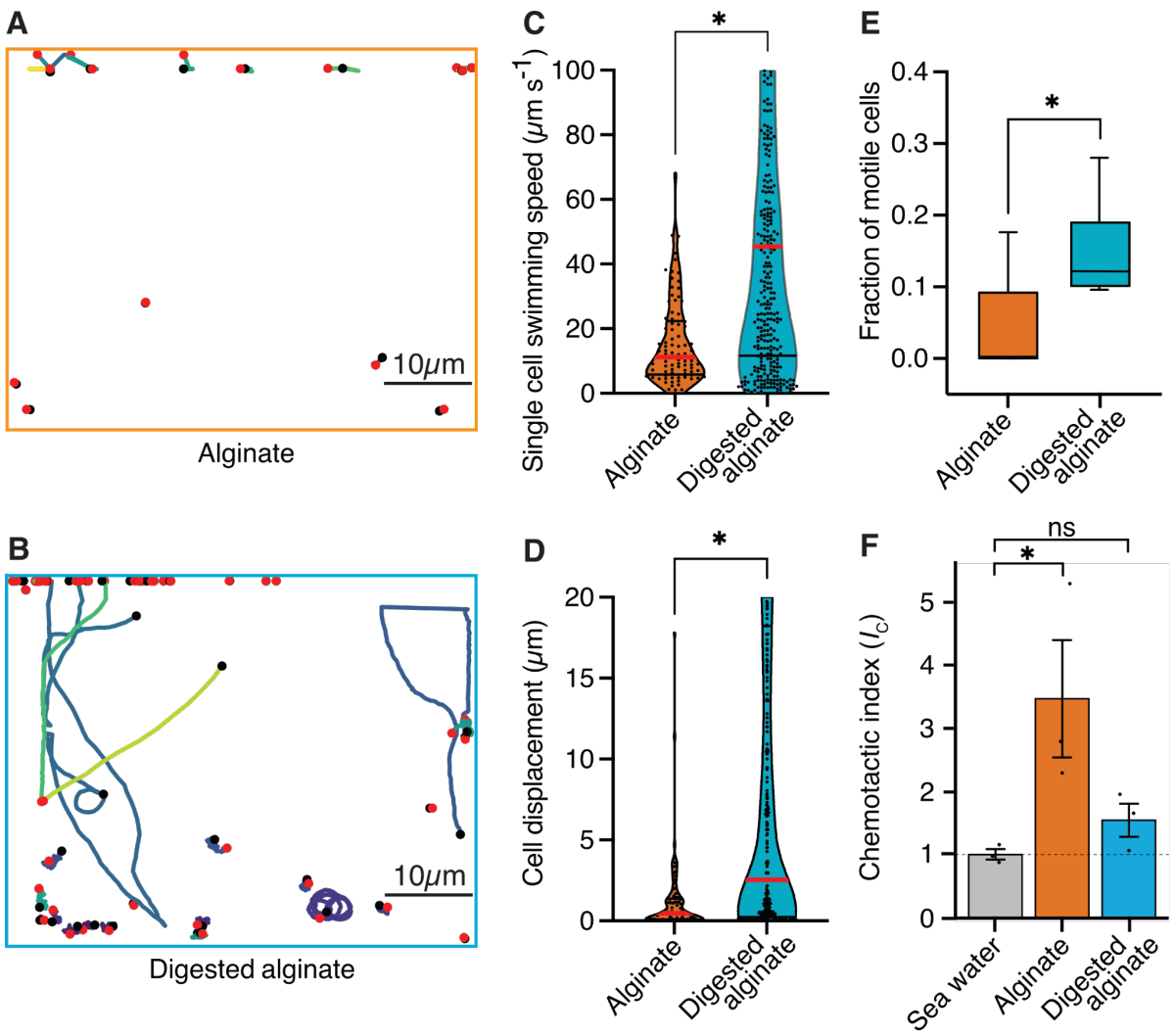

Figure 3. Cells are more motile on digested alginate than alginate and show chemotaxis towards alginate. (A and B) Spatial trajectories of cells supplied with (A) alginate or (B) digested alginate in representative microfluidic growth chambers are shown. Black points mark the starting point of each trajectory, pink points mark the end point of each trajectory, and colored lines mark the trajectories of cells. (C) Distributions of the mean single-cell swimming speeds (Nested t-test, p-value < 0.0007, t = 4.803, df = 10, n_{cells} = 86 vs 375 in $n_{chambers}$ = 5) are shown. (D) Distributions of cell displacement over the course of a trajectory (Nested t-test test, p-value < 0.0131, t = 4.39, df = 10, n_{cells} = 86 vs 375, and $n_{chambers}$ = 5) are shown. In (C) and (D) the red horizontal lines indicate the mean while black lines depict the 25th and 75th quartiles of the distribution. (E) The mean fraction of motile cells in each chamber, where motile cells are defined as cells with displacement greater than 1 μm (Mann-Whitney test on the means of five growth chambers, p-value = 0.034). In C, D, and E, each chamber was considered as an independent replicate. (F) Chemotactic index (I_C) quantified by In Situ Chemotaxis Assay (ISCA) (Tukey multiple comparisons of means, 95% family-wise confidence levels as error bars, p-value < 0.05, n = 3).

258 Asterisks indicate statistically significant differences. See Supplemental Videos S4 and S5 for time-lapse videos
259 of swimming cells.
260
261 **Altered gene expression in central carbon metabolism, enzyme production, secretion and**
262 **transporters, motility, and quorum sensing underlies the late-stage alginate degradation and cell**
263 **dispersal**
264 Next, we sought to elucidate the molecular mechanisms underlying the observed phenomenological
265 disparities between cells cultivated on alginate and digested alginate. Due to the challenge of generating
266 knock-out mutants in natural isolates, we used transcriptomics to investigate the differentially expressed
267 genes of *V. cyclitrophicus* ZF270 under these respective conditions. To obtain a high-quality reference
268 genome of *V. cyclitrophicus* ZF270, we sequenced and assembled a new reference genome using
269 combined short and long read sequencing (BioProject PRJNA991487). We then grew cultures on either
270 alginate or digested alginate until mid-exponential phase. To understand which cellular functions were
271 affected by the expression changes, we first performed differential gene expression analysis using the
272 software DESeq2. Here, genes exhibiting a log2 fold expression change greater than 0.5 or smaller than
273 -0.5 between the two conditions, with a Benjamini-Hochberg(BH)-adjusted *p*-value below 0.01, were
274 considered to be differentially expressed (Table S1). Next, we investigated which KEGG categories
275 were enriched in either genes with increased or decreased expression via Gene Set Enrichment Analysis
276 (GSEA)[23] (Table S2) and found nine categories significantly enriched in genes with increased gene
277 expression on digested alginate, and three categories significantly enriched in genes with decreased
278 gene expression (Fig. 4A).
279
280 Cells growing on digested alginate showed expression changes in parts of the central metabolism and
281 translation, compared to cells growing on alginate. Specifically, two pathways of the central metabolism
282 were significantly enriched in genes with lower expression on digested alginate ("Valine, leucine and
283 isoleucine biosynthesis" and "Propanoate metabolism" with a negative normalized enrichment score
284 (NES), Fig. 4A, S4A and B, Table S3 and S4). We also found the gene set that encodes ribosomal
285 proteins significantly enriched with genes highly expressed on digested alginate (positive NES, Fig. 4A

286 and S4C, Table S5). This implies that cells invest proportionally more of their transcriptome into the
287 production of new proteins, a sign of faster growth[24,25]. Both observations likely relate to the different
288 growth dynamics of *V. cyclitrophicus* ZF270 on digested alginate compared to alginate (Fig. S2A),
289 where cells in digested alginate medium reached their maximal growth rate 7.5 hours earlier and thus
290 showed a shorter lag time (Fig. S2D). As a consequence,, the growth rate at the time of RNA extraction
291 (mid-to-late exponential phase) may have differed, even though the maximum growth rate of cells
292 grown in alginate medium and digested alginate medium were not found to be significantly different
293 (Fig. S2E).
294
295 The expression of transporters and secretion systems was generally increased in cells growing on
296 digested alginate, compared to cells growing on alginate. This includes genes with a function in
297 "Bacterial secretion systems", namely secretion systems I to VI, which mediate protein export through
298 the inner and outer membranes of Gram-negative bacteria (Fig. 4A and S4D, Table S6). Notably, eleven
299 of the thirteen General Secretion Pathway (GSP) genes (part of the type II secretion system) showed
300 1.1 to 3.4-fold increased expression levels on digested alginate (p-values < 0.01, Fig. 4A, Table S8).
301 The GSP is known to facilitate secretion of various extracellular enzymes like chitinases, proteases, and
302 lipases[26,27], therefore, the positive enrichment on digested alginate may be linked to the export of
303 extracellular alginate lyases. The KEGG BRITE category "Secretion system" was also enriched on
304 digested alginate (Fig. 4A and S4D, Table S7). It contains additional genes involved in protein export,
305 implicating them as interesting subjects to further research in their role in protein secretion and cell
306 attachment and detachment during degradation-dispersal cycles of polysaccharide-degrading bacteria.
307 Also, the gene set of transporters and in particular ABC transporters were positively enriched (Fig. 4A,
308 Table S10 and S11). The latter showed enrichment especially in genes related to saccharide, iron, zinc,
309 and phosphate transport (Fig. S4E), which suggests that cells growing on digested alginate invest
310 proportionally more of their transcriptome into uptake of not only saccharides but also essential
311 nutrients like iron, zinc, and phosphate, which may become growth-limiting when degradation products
312 are abundantly available.
313

314 Both motility and quorum sensing genes increased in expression in cells growing on digested alginate.
315 The positive enrichment of the gene set containing bacterial motility proteins aligned with our
316 expectations based on the increase in motile cells that we observed in Figure 3E (Fig. 4A, Table S12).
317 The set of quorum sensing genes was also positively enriched in cells growing on digested alginate
318 (Fig. 4A and S4F, Table S13). This role in dispersal is in agreement with a previous study that showed
319 induction of the quorum sensing master regulator in *V. cholerae* cells during dispersal from biofilms on
320 a similar time scale as here (less than an hour)[28]. Quorum sensing is known to control biofilm formation
321 in the well studied model system *Vibrio cholerae*[29,30] and may also orchestrate the density-dependent
322 dispersal in the presence of degradation products observed in our study, though the particular signaling
323 cues remain to be uncovered. The strong cellular response to the degree of alginate depolymerization
324 was also emphasized by the finding that transcription factor genes were enriched among genes with
325 decreased expression on digested alginate (Fig. 4, Table S14). The set of genes associated to KEGG's
326 beta-lactam resistance category was enriched in genes with increased expression on digested alginate.
327 However, most genes in this gene set are also associated to the KEGG pathways "Transporters",
328 "Quorum sensing", "Chromosome and associated genes", and "Peptidoglycan biosynthesis" and thus
329 the enrichment likely reflects expression changes in these categories and may relate to the difference in
330 growth dynamics (Fig. 4A and S4G, Table S15). Overall, the observed gene expression changes provide
331 insights into the molecular mechanisms underlying the substantial adaptations of *V. cyclitrophicus*
332 ZF270 cells to the polymeric and digested form of alginate.
333

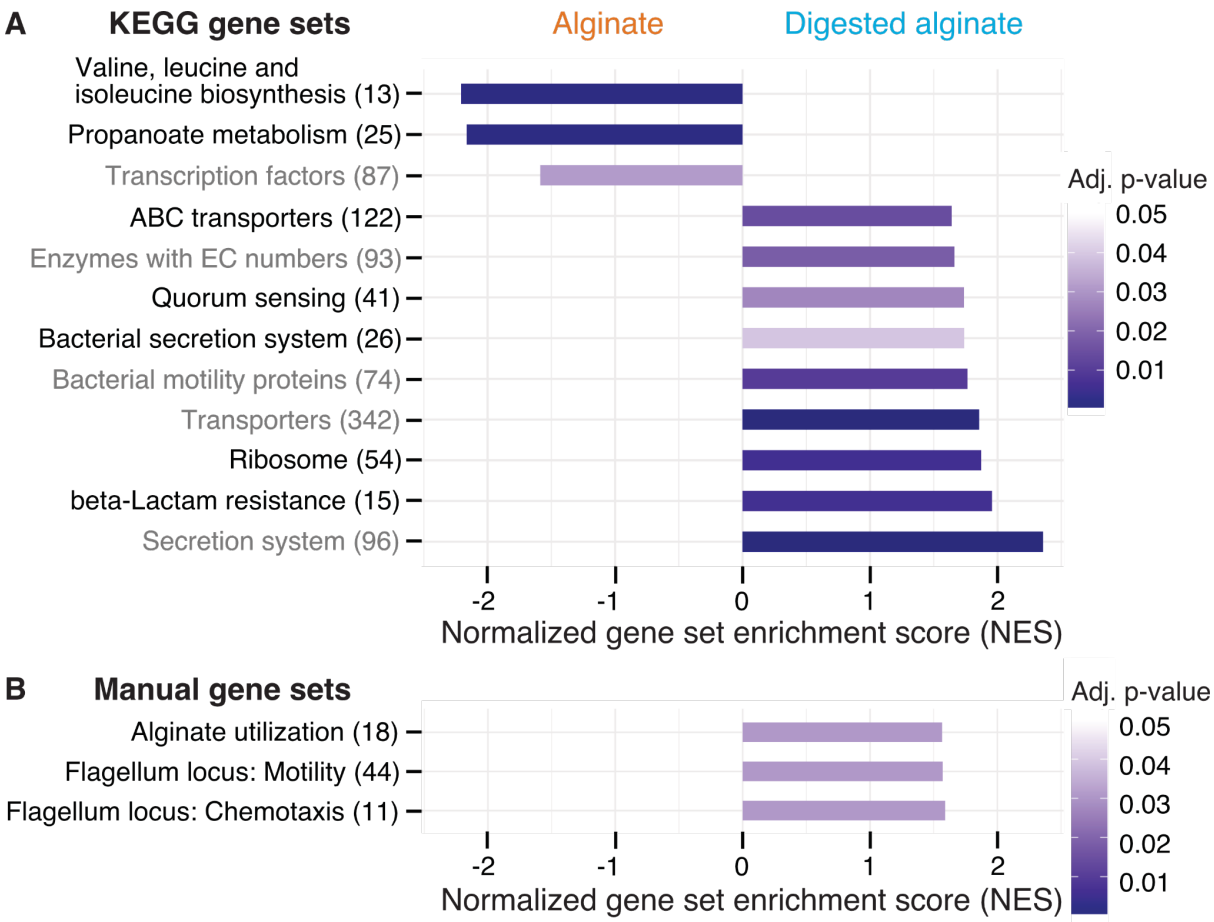

Figure 4. Twelve functional gene sets are enriched in genes with increased or decreased expression in cells grown on digested alginate. Gene set enrichment analysis (GSEA) with (A) all KEGG pathways and KEGG BRITE categories as gene sets or with (B) a custom alginate utilization, flagellar assembly, and flagellum-driven chemotaxis gene set was performed comparing the gene counts of the transcriptome of *V. cyclitrophicus* ZF270 cultures grown on digested alginate and alginate (six replicates each). Gene sets with a positive enrichment score were enriched with genes with higher expression in cells grown on digested alginate relative to cells grown on alginate (BH-adjusted p-value < 0.05), whereas gene sets with negative enrichment scores were significantly enriched with genes with decreased expression on digested alginate. The number in brackets indicates the number of genes with unique K number per gene set (A) and the number of genes per gene set (B) within the *V. cyclitrophicus* ZF270 genome.

Growth on digested alginate is associated with increased expression of alginate catabolism, flagellar motility and chemotaxis genes

For a more fine-grained understanding of the impact of the form of alginate on the alginate catabolism, we investigated specifically the expression of genes involved in alginate degradation, uptake, and

350 catabolism. In the closed genome of *V. cyclitrophicus* ZF270, we identified genes that encode CAZymes
351 responsible for alginate degradation, namely alginate lyase genes from the PL6, PL7, PL15, and PL17
352 family. We identified homologs of alginate transporters (porin *kdgM*, symporter *toaA*, *toaB*, and *toaC*)
353 and metabolic enzymes that shunt into the Entner-Doudoroff pathway (DEHU reductase genes *dehR*,
354 *kdgK*, and *eda*), based on the known genes in the alginate degradation pathway of *Vibrionaceae*[31,32].
355 We found that the expression of most of these genes increased significantly on digested alginate relative
356 to alginate (Fig. 4B, Fig. 5A, S8A, Table S16). Surprisingly, also the expression of most alginate lyase
357 genes increased on digested alginate, especially the expression of secreted alginate lyase genes. This
358 indicates the production of "public" exoenzymes despite the abundance of monomeric and oligomeric
359 degradation products in the digested alginate medium.
360
361 The increased motility of cells observed upon exposure to digested alginate (Fig. 3, Fig. 4A) led us to
362 evaluate the expression of motility- and chemotaxis-associated genes across digested alginate and
363 alginate treatments. As flagella are the main mode of motility in the genus *Vibrio*[33,34], we focused on
364 the expression of flagella-related genes. In the genome of *V. cyclitrophicus* ZF270 we found a gene
365 cluster that encodes most genes involved in flagellar assembly and that was flanked by chemotaxis
366 genes (hereon called flagellar locus, Fig. S8B, and Table S17). Overall, 21/34 flagellar locus genes were
367 differentially expressed (log2 fold change > 0.5, BH-adjusted *p*-value < 0.01) and the majority (90%)
368 of these differentially expressed genes showed increased expression on digested alginate (Fig. 4B). The
369 flagellar genes *flgA*, *fliC*, and *fliH* and the chemotaxis gene *cheW* showed the strongest overexpression
370 (5.4, 3.8, 2.0, and 2.6-fold, respectively). The expression of flagellar biosynthesis genes in *Vibrionacaea*
371 occurs by a cascade of gene expression of four classes of genes (Class I - IV)[35]. We found the expression
372 of the master regulator of the flagellar biosynthesis regulon, the Class I gene *flrA*, to be 1.6-fold
373 increased on digested alginate (BH-adj. *p*-value 3e-19)[36]. The Class II regulatory genes *flrBC*,
374 controlling Class III genes, and *fliA*, controlling Class IV genes, showed 1.5-fold and 1.3-fold increased
375 expression on digested alginate (BH-adj. *p*-value 1e-12 for *flrB*, 2e-39 for *flrC*, 6e-15 for *fliA*) (Fig.
376 5B)[34,37]. These findings suggest that the increased phenotypic motility observed on digested alginate
377 (Fig. 3) is related to the upregulation of flagellar biosynthesis genes. Additionally, the expression of the

flagellum filament, encoded by *fliC* genes of the flagellar locus, was partially increased: *flaD* and *flaC* expression were increased by 3.8 and 1.6-fold, whereas the *flaA* gene was not significantly differentially expressed (BH-adj. *p*-value 7e-37, 2e-19, and 1e-02, respectively) (Fig. 5B, Table S6). This suggests that cells grown on digested alginate have a *flaD*-rich filament composition, which has been shown to alter the swimming and adhesion characteristics of bacterial cells[38,39]. Lastly, we found that most genes involved in chemotaxis and located in the flagellar locus are highly expressed in cells grown on digested alginate (Fig. 5C, Fig. 4B) and likely drive the chemotactic activity of *V. cyclitrophicus* ZF270 during dispersal. Overall, our findings elucidate that cellular responses upon exposure to degradation products manifest in increased expression of genes involved in extracellular alginate breakdown and alginate catabolism as well as flagellar assembly and chemotaxis.

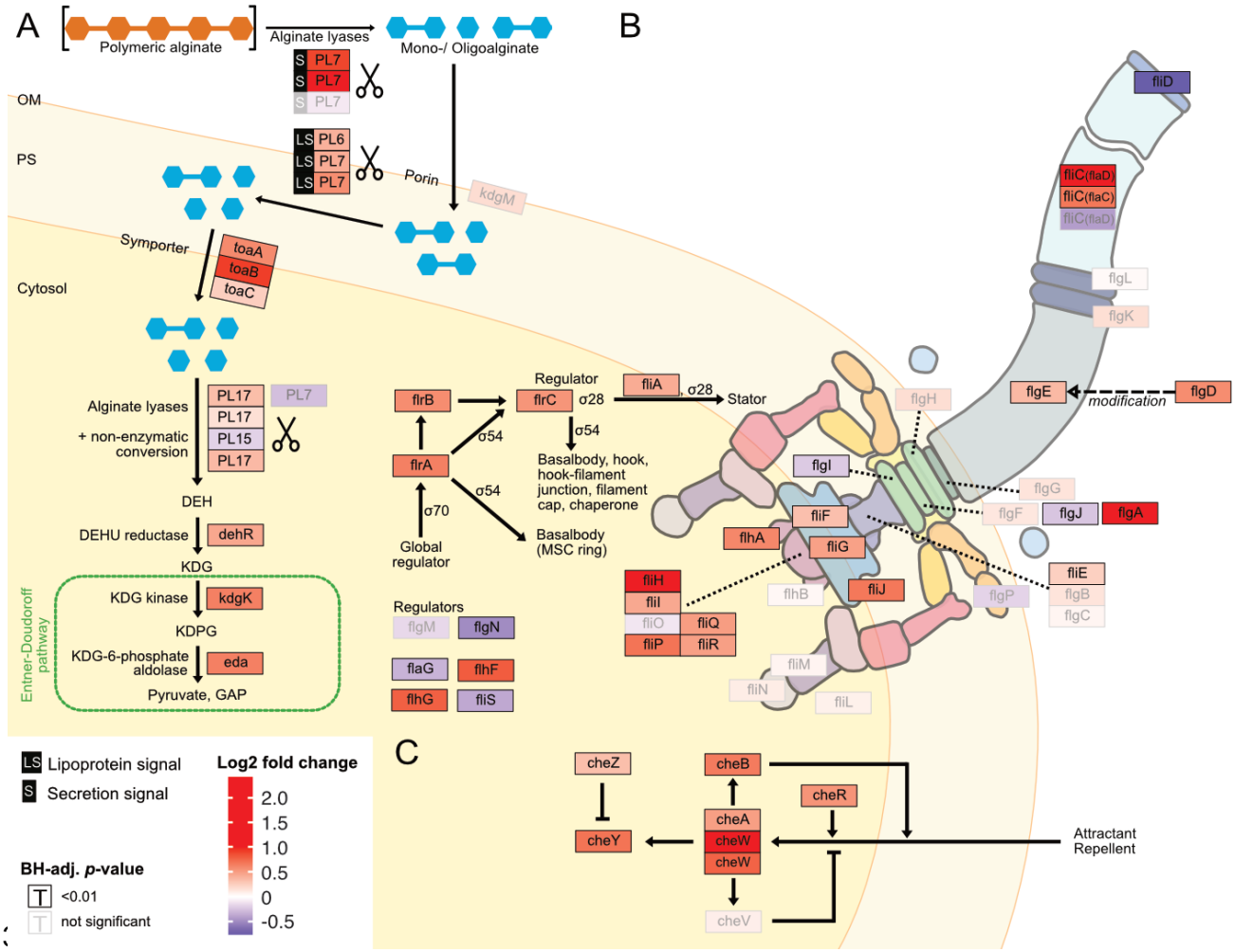

Figure 5. Digested alginate increases expression of genes involved in alginate degradation, uptake and catabolism, as well as flagellar assembly and chemotaxis. Genome-wide differential expression analysis where

391 the log2 fold changes of gene expression on digested alginate compared to alginate is shown for (A) alginate
392 lyases (*PL6, PL7, PL15, PL17,* scissors symbol), transporters (porin *kdgM*, symporter *toaB*, symporter *toaC*), and
393 metabolic enzymes shunting into the Entner-Doudoroff pathway (DEHU reductase *DehR*, *kdgK*, *eda*), (B) genes
394 of the flagellar locus associated with flagellar assembly and (C) adjacent chemotaxis genes. Genes displayed in
395 (B) and (C) are part of the KEGG pathways "Bacterial motility proteins" and "Bacterial chemotaxis". Differential
396 expression analysis was performed to compute the Benjamini-Hochberg-adjusted Wald test *p*-value ("BH-adj. *p*-
397 value", text color and box outline color) and log2 fold change (box fill color) for each gene (box). For better
398 visibility, genes that exhibited a log2 fold gene expression change greater than 1 (i.e., doubling of expression) or
399 less than -1 (i.e., halving of expression) are designated maximum intensity of red or blue, respectively. Genes with
400 BH-adj. *p*-value smaller than 0.01 were considered significantly differentially expressed. In (A), the location of
401 the gene products was based on Figure 1 of Wargacki et al.[31] with the exception of the alginate lyases (*PL6*, *PL7*,
402 *PL15*, *PL17*) which were placed based on their signal peptides (S: extracellular, LS: membrane-embedded, none:
403 cytosolic). In (B) and (C) the gene location and depiction were based on the KEGG pathway "Flagellar assembly"
404 (map02040), "Bacterial chemotaxis" (map02030), and Figure 3 of Rajagopala et al.[40]. Genes without known
405 cellular location were omitted here but displayed in the genomic architecture in Fig. S5. Arrow: activation; dashed
406 arrow: modification; "flat" arrow: inhibition; OM: outer membrane; PM: periplasm; IM: inner membrane; PL:
407 polysaccharide lyase family; *kdgM*: oligogalacturonate-specific outer membrane porin; *toaABC*: oligoalginate
408 symporter; DEH: 4-deoxy-L-erythro-5-hexoseulose uronic acid; *dehR*: DEH reductase; KDG: 2-keto-3-deoxy-
409 gluconate; *kdgK*: KDG kinase; KDPG: 2-keto-3-deoxy-6-phosphogluconate; *eda*: KDG-6-phosphate aldolase;
410 GAP: glyceraldehyde 3-phosphate; ED: Entner-Doudoroff; ns: not significant, i.e. BH-adj. *p*-value > 0.01.
411

412 **Discussion**

413 On Earth organic carbon is mostly present in the form of polysaccharides[1,2], which are often in a
414 particulate state and form a heterogeneous resource landscape. Over the last years, the study of
415 extracellular bacterial degradation of polysaccharides has revealed that bacterial growth on
416 polysaccharides increases with increased cell density, enabling cells to benefit from the exoenzymes
417 and extracellular degradation products of surrounding cells otherwise lost to diffusion ("cooperative
418 growth")[41–43]. However, cells have been observed not only to aggregate on polysaccharide sources, but
419 also to leave them before the source is depleted[13,43]. This cycle of biomass degradation and dispersal

420 has long been discussed in the context of foraging [e.g., 44,45,13,46,47], but the cellular mechanisms that drive
421 the cell dispersal remain unclear.
422
423 Our work links these observations and connects them to the cellular mechanisms that underlie the
424 degradation-dispersal cycles of bacterial degraders, which we see as basal drivers of the biogeochemical
425 processing of polysaccharides in heterogeneous nutrient-scapes. When bacteria encounter a new source
426 of biomass, their local environment likely contains few mono- or oligosaccharides but is rich in
427 polysaccharides which usually require extracellular breakdown (Fig. 6, "Finding a new nutrient
428 source"). General concepts of how bacteria recognize the presence of large biopolymers remain elusive,
429 but it was proposed that "sentry" enzymes are constitutively expressed at a basal level to cleave mono-
430 or oligosaccharides from polysaccharides, which cells can take up and which prime their metabolism
431 for the degradation of the respective polysaccharide[48,49]. It is not known yet how widespread the concept
432 of sentry enzymes may be, but the observation of a constitutively expressed PL7 and PL15 family
433 alginate lyase gene in *Z. galactanivorans*[48] is mirrored in our work by the constant expression of an
434 extracellular PL7 family alginate lyase gene, which may act as sentry enzyme that helps to initiate
435 alginate degradation when cells encounter alginate.
436
437 Growth on polysaccharides has been found to be dependent on the cell density, as increased cell density
438 limits the loss of degradation products and exoenzymes by diffusion[8] (Fig. 6, "Early-stage
439 polysaccharide breakdown"). We found that cells grown on degradation products reach their maximal
440 growth earlier and show increased expression of ribosomal biosynthesis, enzyme secretion, especially
441 of secreted alginate lyases, transporters, quorum sensing and expression changes in the central carbon
442 metabolism. The secretion of alginate lyases might seem surprising and wasteful in a monomer-rich
443 environment. One reason for this observation may be that cells primarily rely on intracellular
444 monosaccharide levels to trigger the upregulation of genes associated with polysaccharide degradation
445 and catabolism, as has previously been observed for *E. coli* across various carbon sources[50,51]. In fact,
446 the majority of carbon sources are sensed by prokaryotes through one-component sensors inside the
447 cell[50]. In the one-component internal sensing scheme, the enzymes and transporters for the use of

448 various carbon sources are expressed at basal levels, which leads to an increase in pathway
449 intermediates upon nutrient availability. The pathway intermediates are sensed by an internal sensor,
450 usually a transcription factor, and lead to the upregulation of transporter and enzyme expression[50,51].
451 This results in a positive feedback loop, which enables small changes in substrate abundance to trigger
452 large transcriptional responses[50,52]. Thus, the presence of alginate breakdown products may likely result
453 in increased expression of all components of the alginate degradation pathway, including the expression
454 of degrading enzymes. As the gene expression analysis was performed on well-mixed cultures in culture
455 medium containing alginate breakdown products, we therefore expect a strong stimulation of alginate
456 catabolism. In a natural scenario, where cells disperse from a polysaccharide hotspot before its
457 exhaustion, the expression of alginate catabolism genes may likely decrease again once the local
458 concentration of breakdown products decreases. However, continued production of alginate lyases
459 could also provide an advantage when encountering a new alginate source and continued production of
460 alginate lyases may thus help cells to prepare for likely future environments. Further investigations of
461 bacterial enzyme secretion in changing nutrient environments and at relevant spatial scales are required
462 to improve our understanding of the regulation of enzyme secretion along nutrient gradients.
463
464 We show that cells respond to the exposure to degradation products with dispersal from dense cell
465 groups by means of increased flagellum-driven swimming (Fig. 6, "Late-stage polysaccharide
466 breakdown"), decreasing their local cell number. This finding matches with previous observations of
467 cells leaving biopolymer particles before they are depleted[13,43]. A plausible explanation for this density-
468 dependent dispersal is that cells in larger groups compete with each other for nutrients and space, while
469 not profiting from cooperative degradation anymore due to the abundance of degradation products.
470 Motility has also been shown to increase the encounter rate of cells with sources of nutrients[53,54],
471 suggesting motility as a strategy that allows cells to escape from the ensuing competition. Previous
472 work in *Caulobacter crescentus* demonstrated that a flagellum knock-out mutant formed larger cell
473 groups, resulting in reduced growth rates due to intercellular competition[4,16]. While it would be
474 interesting to study non-motile mutants of *V. cyclitrophicus* ZF270, the non-tractability of natural
475 isolates makes direct tests of molecular mechanisms difficult. Additionally, subjecting cells separately

476 to the two monomeric units of alginate or oligomers of defined size could improve our understanding
477 of the specific molecules that trigger motility, but this was experimentally not feasible.
478
479 Direct chemotaxis towards polysaccharides may facilitate the search for new polysaccharide sources
480 after dispersal. We found that the presence of degradation products not only induces cell dispersal but
481 also increases the expression of chemotaxis genes. Interestingly, we found that *V. cyclitrophicus* ZF270
482 cells show chemotaxis towards polymeric alginate but not digested alginate. This contrasts with
483 previous findings for bacterial strains degrading the insoluble marine polysaccharide chitin, where
484 chemotaxis was strongest towards chitin oligomers[53], suggesting that oligomers may act as an
485 environmental cue for polysaccharide nutrient sources[55]. However, recent work has shown that certain
486 marine bacteria are attracted to the marine polysaccharide laminarin, and not laminarin oligomers[56].
487 Together with our results, this indicates that chemotaxis towards soluble polysaccharides may be
488 mediated by the polysaccharide molecules themselves. The mechanism of this behavior is yet to be
489 identified, but could be mediated by polysaccharide-binding proteins as have been found in
490 *Sphingomonas* sp. A1 facilitating chemotaxis towards pectin[57]. Direct polysaccharide sensing adds
491 complexity to chemosensing as polysaccharides cannot freely diffuse into the periplasm, which can lead
492 to a trade-off between chemosensing and uptake[58]. Furthermore, most polysaccharides are not
493 immediately metabolically accessible as they require degradation. But direct polysaccharide sensing
494 can also provide certain benefits compared to using oligomers as sensory cues. First, it could enable
495 bacterial strains to preferably navigate to polysaccharide nutrients sources that are relatively
496 uncolonized and hence show little degradation activity. Second, strong chemotaxis towards degradation
497 products could hinder a timely dispersal process as the dispersal then requires cells to travel against a
498 strong attractant gradient formed by the degradation products. Overall, this strategy allows cells to
499 alternate between degradation and dispersal to acquire carbon and energy in a heterogeneous world with
500 nutrient hotspots[44,59–61].
501

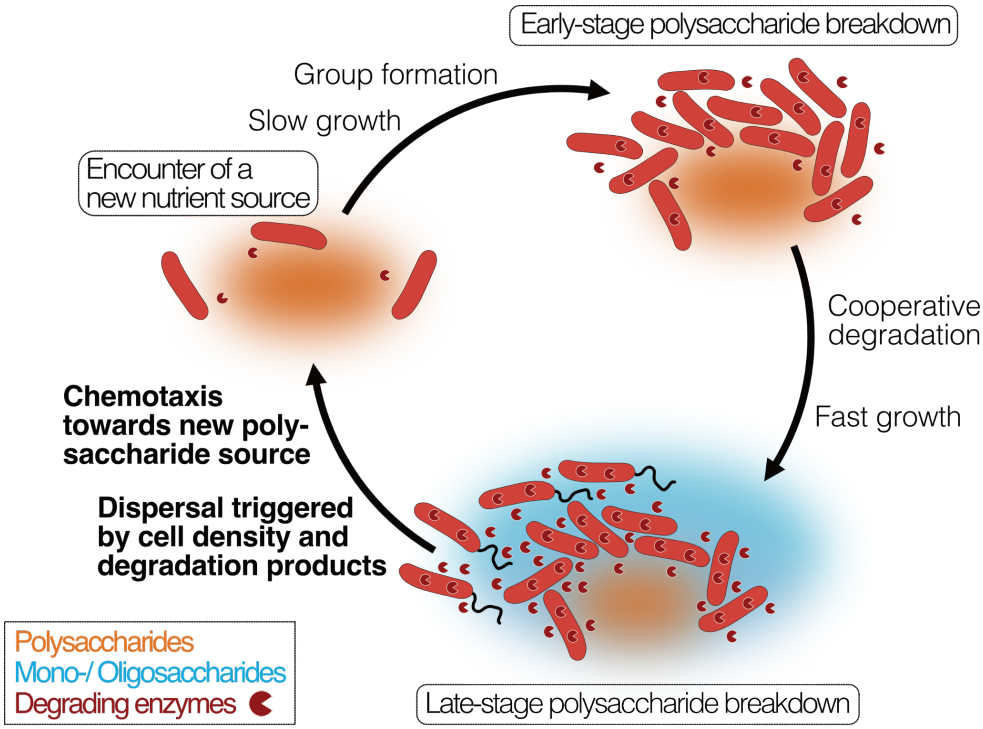

Figure 6. Bacterial growth and regulation on patches of polysaccharides. By integrating our results with previous studies on cooperative growth on the same system, as well as results on dispersal cycles in other systems, we highlight where the specific results of this work add to this framework (bold font). When cells encounter polymer sources, the colonization of the nutrient hotspot may be aided by the basal exoenzyme production of "sentry" enzymes ("Encounter of a new carbon source"). This phase is succeeded by group formation, which enables cells to benefit from exoenzymes of neighboring cells and diffusing degradation products ("Early-stage polysaccharide breakdown"). The following phase includes cooperative extracellular degradation of the polysaccharide source, further increasing the concentration of available degradation products. These degradation products trigger the overexpression of alginate degrading, importing, and catabolizing enzymes, ensuring swift polysaccharide degradation ("Late-stage polysaccharide breakdown"). The increased pool of breakdown products also cues flagellar swimming in a subpopulation of cells and increases the expression of chemotaxis genes. Polymeric alginate acts as chemoattractant towards new polysaccharide sources. Cells and molecules are not drawn to scale. Dark red pie symbols: intracellular and extracellular polysaccharide-degrading enzymes; orange shading: a polymeric carbon source; blue shading: monomeric or oligomeric degradation products.

521 **Conclusion**

522 The heterogeneous landscape of polysaccharide hotspots in natural systems requires bacteria to
523 effectively break down polymeric carbohydrates as well as readily ensure dispersal to new nutrient
524 hotspots. Our findings show that the degree of depolymerization of the polysaccharide influences this
525 decision, altering the growth dynamics, metabolic activity, and motility of cells. Our study also
526 contextualizes the surprising finding that foraging bacteria majorly leave polysaccharide particles
527 before the last third of the particle is consumed[43]. Dispersal from a partially degraded carbon source
528 may serve several purposes: (i) escaping competition that ensues within large cell groups, (ii) ensuring
529 the spread of a part of the clonal population to new environments as bet hedging strategy[47,62], here
530 guided by chemotaxis towards new nutrient hotspots, (iii) preventing whole populations degrading a
531 sinking marine particle or a deposited sediment particle to be buried in depth where nutrient hotspots
532 become sparse[43,63], and/or (iv) increase the genetic variation in bacterial populations[47]. However,
533 dispersal may also occur when a nutrient source offers a surplus of carbon while other essential nutrients
534 become limiting, as the increased expression of iron, zinc, and phosphate transporters in cells grown on
535 digested alginate suggested. These findings emphasize that metabolic molecules can also act as triggers
536 of dispersal, expanding upon the current perspective of dispersal in biofilms as a reaction to dispersal
537 cues like NO, signaling molecules, nutrient starvation, and oxygen starvation[64]. The study of bacterial
538 motility on increasingly complex biomass particles will reveal the role of the nutrient composition of
539 the present nutrient hotspot on the bacterial decision-making. Overall, these new insights into the
540 cellular mechanisms and regulation that drive degradation-dispersal cycles contribute to our
541 understanding of the microbially driven remineralization of biomass, and factors that modulate this
542 process. The open questions of how bacteria sense polysaccharides in their environment, which cell
543 signaling pathways integrate the presence of degradation products in the cellular decision-making of
544 degradation and dispersal, and to what extent cell populations coordinate this decision, present an
545 exciting avenue of further research.

546

547

548

549 **Materials and Methods**

550 *Bacterial strains, media and growth assays*

551 *Vibrio cyclitrophicus* ZF270 (available through Culture Collection Of Switzerland; Accession number:
552 2043) cells were cultured in Marine Broth (DIFCO) and grown for 18 hours at 25 °C. Cells from these
553 cultures were used for growth experiments in Tibbles Rawling (TR) salts minimal medium[65,66]
554 containing either 0.1% (weight/volume) algae-derived alginate (referred to as "alginate") (Sigma
555 Aldrich, CAS-number 9005-38-3) or 0.1% (weight/volume) digested alginate. At these concentrations,
556 both alginate and digested alginate are soluble in the culture medium. The digested alginate was
557 produced by enzymatically digesting 2% alginate with 1 unit ml^{-1} of alginate lyase (Sigma Aldrich,
558 CAS-number 9024-15-1) at 37 °C for 48 hours. Carbon sources were prepared in nanopure water and
559 filter sterilized using 0.40 µm Surfactant-Free Cellulose Acetate filters (Corning, USA). Well-mixed
560 batch experiments in alginate or digested alginate medium were performed in 96-well plates (Greiner
561 Bio) and growth dynamics were measured using a microwell plate reader (Biotek, USA). Plate reader
562 assays were initiated as described previously[67]. Briefly, 1 ml from a culture grown for 18 h on Marine
563 broth was centrifuged at 5000 g in 1.5 ml microfuge tubes for 5 minutes. The supernatant was discarded
564 and the cell pellet was subjected to two rounds of washing with the basal TR salts medium. The cell-
565 pellet was then resuspended in 1 ml of TR salts medium and 5 µl of this suspension inoculated into 195
566 µl TR medium with either carbon source ($\sim 10^5$ colony forming units (CFUs ml^{-1}) in a 96-well plate
567 (Greiner Bio). The optical density (600 nm) was then measured every 15 minutes for 40 hours. All
568 measurements had six biological replicates.

569

570 *Alginate oligosaccharide measurements*

571 Oligosaccharide measurements were performed using liquid chromatography time of flight mass
572 spectrometry (LC-QTOF-MS). Samples were prepared by diluting 1:20 in milliQ water and 5 µL of
573 sample was injected per measurement. Chromatographic separation was performed using an Agilent
574 1290 stack, using an Agilent HILIC-Z column (2.7 µm particles, 2.1 x 50 mm). Mobile phase A
575 contained 10% acetonitrile (Fisher Scientific) and 0.1% medronic acid (Agilent), and Mobile phase B

576 contained 90% acetonitrile and 0.1% medronic acid. The separation was performed as follows: Mobile
577 phase B 100% for 1 minute, gradient to 30% phase B over 3 minutes, 30% phase B for 30 seconds, and
578 equilibration of 100% phase B for 5 minutes. The flow rate was 400 μL min^{-1} at 30 °C. Samples were
579 measured using an Agilent 6520 mass spectrometer in negative mode, in 4 GHz high-resolution mode.
580 Data analysis was performed in Agilent Quantitative Analysis software.
581
582 *Microfluidics and time-lapse microscopy*
583 Microfluidic experiments and microscopy were performed as described previously[15,16,68]. Cells were
584 imaged within chambers of a PDMS (Sylgard-Dow) microfluidic chip that ranged in size from 60-120
585 × 60 × 0.56 μm ($l \times b \times h$). Within these chambers, cells can attach to the glass surface and experience
586 the medium that diffuses through lateral flow channels. Imaging was performed using IX83 inverted
587 microscope systems (Olympus, Japan) with automated stage controller (Marzhauser Wetzlar,
588 Germany), shutter, and laser-based autofocus system (Olympus ZDC 2). Chambers were imaged in
589 parallel on the same PDMS chip, and phase-contrast images of each position were taken every 8 or 10
590 minutes. The microscopy unit and PDMS chip were maintained at 25 °C using a cellVivo microscope
591 incubation system (Pecon GmbH).
592
593 *Viscosity of the alginate and digested alginate solution*
594 We measured the viscosity of alginate solutions using shear rheology measurements. We use a 40 mm
595 cone-plate geometry (4° cone) in a Netzsch Kinexus Pro+ rheometer. 1200 uL of sample was placed on
596 the bottom plate, the gap was set at 150 um and the sample trimmed. We used a solvent trap to avoid
597 sample evaporation during measurement. The temperature was set to 25°C using a Peltier element. We
598 measure the dynamic viscosity over a range of shear rates = 0.1 – 100 s-1. We report the viscosity of
599 each solution as the average viscosity measured over the shear rates 10 – 100 s-1, where the shear-
600 dependence of the viscosity was low.
601 We measured the viscosity of 0.1% (w/V) alginate dissolved in TR media, which was 1.03 +/- 0.01
602 mPa·s (reporting the mean and standard deviation of three technical replicates.). The viscosity of 0.1%

603 digested alginate in TR media was found to be 0.74+/-0.01 mPa·s. This means that the viscosity of
604 alginate in our microfluidic experiments is 36% higher than of digested alginate, but the viscosities are
605 close to those expected of water (0.89 mPa·s at 25 degree celsius according to Berstad and colleagues
606 (1988)[18]).
607
608 *Motility assays*
609 Cells were grown for 10 hours in Marine Broth (DIFCO) after which 10 µl of culture was used to
610 inoculate culture tubes (Greiner) containing 5 ml of TR medium with either 0.1% alginate or 0.1%
611 digested alginate. After 6 hours of growth at 25 °C, 2 µl of cell suspension was inoculated into
612 microfluidic growth chambers. Cells within six replicate chambers were then imaged with the phase-
613 contrast channel at a high frame rate (125 Hz, i.e., frames s^{-1}) using the same microscopy setup described
614 above.
615
616 *Chemotaxis assays*
617 To assess whether polymeric alginate and digested alginate attract *Vibrio cyclitrophicus* ZF270, we
618 used the *In Situ* Chemotaxis Assay[21,22] (ISCA), a microfluidic device consisting of a 5 × 5 array of
619 microwells that can be individually loaded with solutions of different chemicals (110 µl each). Once
620 the ISCA is deployed in an aqueous environment, the chemicals diffuse out of the wells through a small
621 port, creating chemical gradients which will guide chemotactic bacteria inside the wells of the
622 device[21,22]. *Vibrio cyclitrophicus* ZF210 was plated on Marine Agar (BD Difco) from a glycerol stock
623 and grown for 16 h at 27 °C. A single colony was then incubated in 10% Marine Broth (BD Difco) in
624 0.22-µm filtered artificial seawater (Instant Ocean, Spectrum Brands) and grown overnight at 27 °C and
625 180 rpm. The culture was diluted down to 1 x 10^6 cells ml^{-1} in 0.22 µm filtered artificial seawater (Instant
626 Ocean, Spectrum Brands) to perform the chemotaxis experiment. Both chemoattractants (alginate and
627 digested alginate) were diluted in sterile seawater (35 g l^{-1}; Instant Ocean, Spectrum Brands) at a final
628 concentration of 0.1% and then filtered with a 0.2 µm filter (Millipore) to remove particles and potential
629 contaminants. Within the ISCA, one full row of five wells was used per chemoattractant as technical
630 replicates. The chemoattractants were injected in triplicate ISCA with a sterile 1 ml syringe (Codau)

631 and needle (27 G, Henke Sass Wolf). A last row containing 0.2 µm-filtered seawater acted as negative
632 control accounting for cells swimming in the device by random motility only. Experiments were
633 conducted by incubating the ISCAs for 1 h in the diluted *Vibrio cyclitrophicus* ZF270 culture. Upon
634 time completion, a sterile syringe and needle were used to retrieve the content of the wells and
635 transferred to 1 ml microfuge tubes resulting in a pooling of a row of 5 wells containing the same
636 sample. Sample staining was performed with SYBR Green I (Thermo Fisher) and the chemotactic
637 response was quantified by counting cells using flow cytometry. The strength of the chemotactic
638 response was determined by the mean chemotactic index (I_C), defined as the ratio of the number of cells
639 found in each chemoattractant to the number of cells in control wells containing filtered seawater (so
640 that attraction corresponds to $I_C > 1$).
641
642 *Culturing and harvesting cells for transcriptomics*
643 Cells were grown for 18 hours in Marine Broth (DIFCO) after which 1 ml of culture was centrifuged at
644 5000 g in 1.5 ml microfuge tubes for 5 minutes. The supernatant was discarded and the cell pellet was
645 subjected to two rounds of washing with the basal TR salts medium. The cell pellet was then
646 resuspended in 1 ml of TR salts medium and 250 µl of this suspension were used to inoculate 100 ml
647 flasks (Schott-Duran) containing 10 ml of TR medium with either 0.1% alginate or 0.1% digested
648 alginate. This was done in parallel for six flasks. Once cultures in the flasks reached mid-exponential
649 phase (10 hours and 15 hours after inoculation for digested alginate and alginate, respectively) and had
650 approximately the same OD (0.39 for digested alginate and 0.41 for alginate), 2 ml of cultures were
651 harvested for RNA extraction. Samples were stabilized with the RNprotect reagent (Qiagen) and RNA
652 was extracted using the RNeasy mini kit (Qiagen).
653
654 *Sequencing and gene annotation of Vibrio cyclitrophicus* ZF270
655 Long read sequencing using the Oxford Nanopore Platform (Long read DNA sequencing kit) and short
656 read sequencing using the Illumina platform (Illumina DNA Prep kit and IDT 10bp UDI indices, and
657 sequenced on an Illumina NextSeq 2000 producing 2x151bp reads) was performed by the Microbial
658 Genome Sequencing Center, Pittsburgh, USA (MiGS), to create a new closed reference genome of *V.*

659 *cyclitrophicus* ZF270 (BioProject PRJNA991487). Annotation of this genome was done with RASTtk
660 (v2.0, Rapid Annotation using Subsystem Technology tool kit[69]). Additionally, KEGG Ontology
661 identifiers ("K numbers") were annotated with BlastKOALA (v2.2)[70]. Dedicated annotation of alginate
662 lyase genes was performed by homology search for proteins belonging to the PL5, PL6, PL7, PL14,
663 PL15, PL17, PL18, PL31, PL36, or PL39 family[71] by dbCAN2 (v9.0)[72]. Enzymes for alginate transport
664 and metabolism were identified by BLASTn-search[73,74] of gene sequences of *Vibrio splendidus* 12B01,
665 which were previously identified as minimum genetic prerequisites for alginate utilization and enabled
666 alginate degradation when cloned into *E. coli*[31].
667
668 *Location prediction of alginate lyases*
669 Signal peptides were annotated using SignalP (v.5.0)[75], and LipoP (v.1.0)[76]. SignalP discriminated
670 between 1) Sec/SPI: "standard" secretory signal peptides transported by the Sec translocon and cleaved
671 by Signal Peptidase I (SPI), 2) Sec/SPII: lipoprotein signal peptides transported by the Sec translocon
672 and cleaved by Signal Peptidase II (SPII), and 3) Tat/SPI: Tat signal peptides transported by the Tat
673 translocon and cleaved by SPI. LipoP discriminates between 1) SPI: signal peptide, 2) SpII: lipoprotein
674 signal peptide, and 3) TMH: n-terminal transmembrane helix. All predictions were in agreement, apart
675 from one PL7 (gene 1136176.5.peg.4375) which was predicted by LipoP as cytoplasmic and by SignalP
676 as equally likely cytoplasmic as containing a lipoprotein signal peptide.
677
678 *Transcriptomic analysis: Sequencing, pre-processing, differential expression analysis, and functional*
679 *analysis*
680 Sequencing (12 M reads, 2 x 50 bp) of the isolated RNA was performed by MiGS after rRNA depletion
681 using RiboZero Plus (Ilumina). cDNA libraries were prepared using an Illumina DNA Prep kit and IDT
682 10 bp UDI indices, and sequenced on an Illumina NextSeq 2000. Preprocessing of the raw reads was
683 carried out as follows: Quality control was performed with FastQC (v0.11.9)[77] and reads were trimmed
684 with Trimmomatic (v0.38)[78]; the high-quality reads were mapped to the reference genome (described
685 above) with Bowtie2 (v2.3.5.1)[79]; binarization, sorting, and indexing were done with Samtools
686 (v1.10)[80]; gene counts were computed with the featureCount function of Subread (v2.0.1)[81].

687 Differential expression analysis was performed with DESeq2 (v1.30.1)[82]. In brief, DESeq2 normalizes
688 the raw read counts with normalization factors ("size factors") to account for differences in sequencing
689 depth between samples. Subsequently, gene-wise dispersion estimates are computed for each gene
690 separately using maximum likelihood, and then shrunk toward the values predicted by the dispersion-
691 mean dependence curve to obtain final dispersion values. Finally, DESeq2 fits a negative binomial
692 model to the read counts and performs significance testing using the Wald test. Here reported *p*-values
693 result from the Wald test of read counts from the digested alginate condition compared to the alginate
694 condition and were adjusted for multiple testing by Benjamini-Hochberg correction[83] as implemented
695 in the p.adjust function of base R (v4.1.2). The reported log2 fold changes indicate the log2(DESeq2-
696 normalised reads in digested alginate condition / DESeq2-normalised reads in alginate condition) for
697 each gene.
698 Visualization of gene maps was performed in R with the ggplot2 package (v3.4.0) and the extension
699 gggenes (v0.4.1) by David Wilkins.
700 For systematic functional analysis we performed gene set enrichment analysis (GSEA)[23] using the fgsea
701 function of the fgsea package (v1.20.0) with minimal number of unique genes per gene set "minSize"
702 = 5 and number of permutations "nPermSimple" = 1000000. In brief, GSEA takes the full gene list
703 ranked by log2 fold change and annotated with K numbers as input and determines whether the member
704 genes of any KEGG pathway are randomly distributed throughout the ranked gene list or whether they
705 are primarily found at the top or bottom[23]. This is quantified by the enrichment score (ES), which
706 corresponds to a weighted Kolmogorov-Smirnov-like statistic. The ES of each gene set is normalized
707 to the mean enrichment of random samples of the same size to account for the size of the set, yielding
708 the normalized enrichment score (NES). To estimate the significance level of the enrichment score, the
709 *p*-value of the observed enrichment score is calculated relative to a null distribution that was computed
710 from permuted data. The estimated significance level was adjusted to account for multiple hypothesis
711 testing. As gene sets we chose all KEGG pathways and KEGG BRITE categories (as noted in Table S1
712 in column "KEGG_pathway") within all genes of *V. cyclitrophicus* ZF270 annotated with a KEGG
713 Ontology identifier ("K number"). Visualization of differential expression levels in KEGG pathways
714 was performed with the R package pathview (v1.35.0)[84]. We also formed gene sets of the genes

associated with alginate utilization (see "*Sequencing and gene annotation of Vibrio cyclitrophicus* ZF270", Table S16), of the genes of the flagellar locus that map to the KEGG pathways "Bacterial motility proteins", and of the genes of the flagellar locus that map to the KEGG pathways "Bacterial chemotaxis" (as noted in Table S17) within all genes of *V. cyclitrophicus* ZF270.

Image analysis

Cells within microscopy images were segmented and tracked using ilastik (v1.3) ("pixel classification workflow" and "tracking with probabilities workflow"). Phase contrast images were used for alignment, segmentation, tracking and linking. Images were cropped at the boundaries of each microfluidic chamber. The lineage identity of each single cell was assigned by ilastik's tracking plugin and visualized by coloring the segmented cells, respectively. The growth rate of each cell was computed as the change of cell area over time, i.e., via a linear regression of the single-cell area over the time between consecutive cell divisions, based on ilastik's segmentation and tracking output. Cells that were tracked over less than three frames were excluded. Measurement of swimming speeds and displacement of cells was performed using ilastik (v1.4), ImageJ (v2.3) and Trackmate (v7.5.2). Briefly, cell-segmentation ("pixel classification workflow" in ilastik) and tracking ("animal tracking workflow" in ilastik) were performed using the high frame rate phase contrast images in ilastik (v1.4). Cell trajectories and properties were then computed using the output of the ilastik workflow in Trackmate.

Dispersal analysis

For the analysis on the dispersal of cells (Fig. 2), we computed the cell number as the total number of cells within a microfluidic chamber. The change in the number of cells was computed by subtracting the number of cells before the medium switch (i.e., average number of cells between t = 1.9 to 2.1 h) from the number of cells after the medium switch (i.e., average number of cells between t = 3.9 to 5.5 h).

Datasets and statistical analysis

742 All batch experiments were replicated 3 to 6 times. Growth curves were analyzed in Python (v3.7) using
743 the *Amiga* package (v1.1.0)[85] and GraphPad Prism (v8, GraphPad Software). The microscopy dataset
744 consisted of eight chambers each, corresponding to the eight replicates shown in Figure 1 and Figure 2.
745 These were grouped into two biological replicates wherein each biological replicate was fed by media
746 through a unique channel in a microfluidic chip. Cells with negative growth rates were excluded from
747 the analysis after visual curation, as they represented artifacts, mistakes in segmentation or linking
748 during the tracking process, or non-growing deformed cells. Each chamber was treated as an
749 independent replicate. Comparisons were considered statistically significant when $p < 0.05$ or when the
750 False Discovery Rate (FDR)-corrected q was smaller than 0.05. FDR corrections were applied when
751 multiple t tests were performed for the same dataset. Measures of effect size are represented by the R^2
752 or eta^2 value. All statistical analyses were performed in GraphPad Prism v9.0 (GraphPad Software,
753 USA), R v4.1.2, RStudio v1.1.463 (Posit, USA).
754
755 **Acknowledgements:** We thank past and present members of the Microbial Systems Ecology group for
756 feedback. This research was supported by an ETH fellowship and a Marie Skłodowska-Curie Actions
757 for People COFUND program fellowship (FEL-37-16-1) to GD; an ETH Career Seed Grant to GD
758 (FEL-14 18-1), the Simons Foundation Collaboration on Principles of Microbial Ecosystems (PriME,
759 #542379 and #542395) to MA and RS; and by ETH Zurich and Eawag.
760
761 **Data Availability:** Sequencing data is available on NCBI, BioProject PRJNA991487, upon publication.
762 All further data and code is deposited on ERIC Open (https://opendata.eawag.ch/,
763 https://doi.org/10.25678/0008MH), available upon publication. Code will also be made publicly
764 accessible on https://github.com/Microbial-Systems-Ecology/publications upon publication.
765
766 **Competing interests:** The authors declare no competing interests.
767
768 **Author Contributions:** GD, AS, JS, and JK conceived the research along with MA. GD designed and
769 performed the experiments. AS developed and implemented the algorithms to compute single-cell

growth rates and visualize lineage identities from segmented and tracked cells. AS analyzed and visualized the RNA-seq data. JK conceived and implemented the cell dispersal analysis. EC conducted the ISCA experiment. SP carried out the mass spectrometry measurements. AS and GD analyzed the data with inputs from JK, JS, CM, MA, and RS. AS wrote the manuscript with inputs from GD, OS, MA, JK, JS, EC, SP, CM, and RS.

Citations:

1. BeMiller JN. 4 - Polysaccharides: Occurrence, Structures, and Chemistry. In: BeMiller JN, ed. *Carbohydrate Chemistry for Food Scientists (Third Edition)*. AACC International Press; 2019:75-101. doi:10.1016/B978-0-12-812069-9.00004-2

2. Reintjes G, Arnosti C, Fuchs B, Amann R. Selfish, sharing and scavenging bacteria in the Atlantic Ocean: a biogeographical study of bacterial substrate utilisation. *ISME J*. 2019;13(5):1119-1132. doi:10.1038/s41396-018-0326-3

3. Ratzke C, Gore J. Self-organized patchiness facilitates survival in a cooperatively growing Bacillus subtilis population. *Nature Microbiology*. 2016;1(5):16022. doi:10.1038/nmicrobiol.2016.22

4. Povolo VR, D'Souza GG, Kaczmarczyk A, Stubbusch AK, Jenal U, Ackermann M. Extracellular appendages govern spatial dynamics and growth of Caulobacter crescentus on a prevalent biopolymer. *bioRxiv*. Published online January 1, 2022:2022.06.13.495907. doi:10.1101/2022.06.13.495907

5. Westrich JR, Griffin DW, Westphal DL, Lipp EK. Vibrio Population Dynamics in Mid-Atlantic Surface Waters during Saharan Dust Events. *Frontiers in Marine Science*. 2018;5. https://www.frontiersin.org/articles/10.3389/fmars.2018.00012

6. Takemura A, Chien D, Polz M. Associations and dynamics of Vibrionaceae in the environment, from the genus to the population level. *Frontiers in Microbiology*. 2014;5. https://www.frontiersin.org/articles/10.3389/fmicb.2014.00038

7. Schwartzman JA, Ebrahimi A, Chadwick G, et al. Bacterial growth in multicellular aggregates leads to the emergence of complex life cycles. *Current Biology*. 2022;32(14):3059-3069.e7. doi:10.1016/j.cub.2022.06.011

8. D'Souza G, Ebrahimi A, Stubbusch A, et al. Cell aggregation is associated with enzyme secretion strategies in marine polysaccharide-degrading bacteria. *ISME J*. Published online February 22, 2023. doi:10.1038/s41396-023-01385-1

9. Wang X, Liu J, Liang J, Sun H, Zhang XH. Spatiotemporal dynamics of the total and active Vibrio spp. populations throughout the Changjiang estuary in China. *Environmental Microbiology*. 2020;22(10):4438-4455. doi:10.1111/1462-2920.15152

10. Wong TY, Preston LA, Schiller NL. Alginate Lyase: Review of Major Sources and Enzyme Characteristics, Structure-Function Analysis, Biological Roles, and Applications. *Annual Review of Microbiology*. 2000;54(1):289-340. doi:10.1146/annurev.micro.54.1.289

11. Mabeau S, Kloareg B. Isolation and Analysis of the Cell Walls of Brown Algae: Fucus spiralis, F. ceranoides, F. vesiculosus, F. serratus, Bifurcaria bifurcata and Laminaria digitata. *Journal of Experimental Botany*. 1987;38(9):1573-1580. doi:10.1093/jxb/38.9.1573

12. Hunt DE, David LA, Gevers D, Preheim SP, Alm EJ, Polz MF. Resource Partitioning and Sympatric Differentiation Among Closely Related Bacterioplankton. *Science*. Published online May 23, 2008. doi:10.1126/science.1157890

13. Yawata Y, Cordero OX, Menolascina F, Hehemann JH, Polz MF, Stocker R. Competition–dispersal tradeoff ecologically differentiates recently speciated marine bacterioplankton populations. *Proc Natl Acad Sci USA*. 2014;111(15):5622-5627. doi:10.1073/pnas.1318943111

14. Huang L, Zhou J, Li X, Peng Q, Lu H, Du Y. Characterization of a new alginate lyase from newly isolated *Flavobacterium* sp. S20. *Journal of Industrial Microbiology and Biotechnology*. 2013;40(1):113-122. doi:10.1007/s10295-012-1210-1

15. Dal Co A, van Vliet S, Kiviet DJ, Schlegel S, Ackermann M. Short-range interactions govern the dynamics and functions of microbial communities. *Nat Ecol Evol*. 2020;4(3):366-375. doi:10.1038/s41559-019-1080-2

16. D'Souza GG, Povolo VR, Keegstra JM, Stocker R, Ackermann M. Nutrient complexity triggers transitions between solitary and colonial growth in bacterial populations. *ISME J*. 2021;15(9):2614-2626. doi:10.1038/s41396-021-00953-7

17. D'Souza G, Schwartzman J, Keegstra J, et al. Interspecies interactions determine growth dynamics of biopolymer-degrading populations in microbial communities. *Proc Natl Acad Sci U S A*. 2023;120(44):e2305198120. doi:10.1073/pnas.2305198120

18. Berstad DA, Knapstad B, Lamvik M, Skjølsvik PA, Tørklep K, Øye HA. Accurate measurements of the viscosity of water in the temperature range 19.5–25.5°C. *Physica A: Statistical Mechanics and its Applications*. 1988;151(2-3):246-280. doi:10.1016/0378-4371(88)90015-5

19. Zöttl A, Yeomans JM. Enhanced bacterial swimming speeds in macromolecular polymer solutions. *Nat Phys*. 2019;15(6):554-558. doi:10.1038/s41567-019-0454-3

20. BERG HC, TURNER L. Movement of microorganisms in viscous environments. *Nature*. 1979;278(5702):349-351. doi:10.1038/278349a0

21. Lambert BS, Raina JB, Fernandez VI, et al. A microfluidics-based in situ chemotaxis assay to study the behaviour of aquatic microbial communities. *Nat Microbiol*. 2017;2(10):1344-1349. doi:10.1038/s41564-017-0010-9

22. Clerc EE, Raina JB, Lambert BS, Seymour J, Stocker R. In Situ Chemotaxis Assay to Examine Microbial Behavior in Aquatic Ecosystems. *JoVE*. 2020;(159):e61062. doi:10.3791/61062

23. Subramanian A, Tamayo P, Mootha VK, et al. Gene set enrichment analysis: a knowledge-based approach for interpreting genome-wide expression profiles. *Proc Natl Acad Sci U S A*. 2005;102(43):15545-15550. doi:10.1073/pnas.0506580102

24. Wei Y, Lee JM, Richmond C, Blattner FR, Rafalski JA, LaRossa RA. High-Density Microarray-Mediated Gene Expression Profiling of *Escherichia coli*. *J Bacteriol*. 2001;183(2):545-556. doi:10.1128/JB.183.2.545-556.2001

25. Gifford SM, Sharma S, Booth M, Moran MA. Expression patterns reveal niche diversification in a marine microbial assemblage. *ISME J*. 2013;7(2):281-298. doi:10.1038/ismej.2012.96

26. Johnson TL, Fong JC, Rule C, Rogers A, Yildiz FH, Sandkvist M. The Type II Secretion System Delivers Matrix Proteins for Biofilm Formation by Vibrio cholerae. *J Bacteriol*.

852 2014;196(24):4245-4252. doi:10.1128/JB.01944-14

853 27. Sikora AE. Proteins Secreted via the Type II Secretion System: Smart Strategies of Vibrio
854 cholerae to Maintain Fitness in Different Ecological Niches. Heitman J, ed. *PLoS Pathog*.
855 2013;9(2):e1003126. doi:10.1371/journal.ppat.1003126

856 28. Singh PK, Bartalomej S, Hartmann R, et al. Vibrio cholerae Combines Individual and Collective
857 Sensing to Trigger Biofilm Dispersal. *Current Biology*. 2017;27(21):3359-3366.e7.
858 doi:10.1016/j.cub.2017.09.041

859 29. Jemielita M, Wingreen NS, Bassler BL. Quorum sensing controls Vibrio cholerae multicellular
860 aggregate formation. Storz G, ed. *eLife*. 2018;7:e42057. doi:10.7554/eLife.42057

861 30. Waters CM, Lu W, Rabinowitz JD, Bassler BL. Quorum sensing controls biofilm formation in
862 Vibrio cholerae through modulation of cyclic di-GMP levels and repression of vpsT. *J Bacteriol*.
863 2008;190(7):2527-2536. doi:10.1128/JB.01756-07

864 31. Wargacki AJ, Leonard E, Win MN, et al. An Engineered Microbial Platform for Direct Biofuel
865 Production from Brown Macroalgae. *Science*. 2012;230502(January):308-314.

866 32. Zhang L, Li X, Zhang X, Li Y, Wang L. Bacterial alginate metabolism: an important pathway for
867 bioconversion of brown algae. *Biotechnol Biofuels*. 2021;14(1):158. doi:10.1186/s13068-021-
868 02007-8

869 33. Khan F, Tabassum N, Anand R, Kim YM. Motility of Vibrio spp.: regulation and controlling
870 strategies. *Appl Microbiol Biotechnol*. 2020;104(19):8187-8208. doi:10.1007/s00253-020-10794-
871 7

872 34. Echazarreta MA, Klose KE. Vibrio Flagellar Synthesis. *Front Cell Infect Microbiol*. 2019;9:131.
873 doi:10.3389/fcimb.2019.00131

874 35. Prouty MG, Correa NE, Klose KE. The novel sigma54- and sigma28-dependent flagellar gene
875 transcription hierarchy of Vibrio cholerae. *Mol Microbiol*. 2001;39(6):1595-1609.
876 doi:10.1046/j.1365-2958.2001.02348.x

877 36. Klose KE, Mekalanos JJ. Differential Regulation of Multiple Flagellins in *Vibrio cholerae*. *J*
878 *Bacteriol*. 1998;180(2):303-316. doi:10.1128/JB.180.2.303-316.1998

879 37. Srivastava D, Hsieh ML, Khataokar A, Neiditch MB, Waters CM. Cyclic di-GMP inhibits Vibrio
880 cholerae motility by repressing induction of transcription and inducing extracellular
881 polysaccharide production. *Mol Microbiol*. 2013;90(6):1262-1276. doi:10.1111/mmi.12432

882 38. Kim SY, Thanh XTT, Jeong K, et al. Contribution of six flagellin genes to the flagellum
883 biogenesis of Vibrio vulnificus and in vivo invasion. *Infect Immun*. 2014;82(1):29-42.
884 doi:10.1128/iai.00654-13

885 39. Nedeljković M, Sastre DE, Sundberg EJ. Bacterial Flagellar Filament: A Supramolecular
886 Multifunctional Nanostructure. *Int J Mol Sci*. 2021;22(14):7521. doi:10.3390/ijms22147521

887 40. Rajagopala SV, Titz B, Goll J, et al. The protein network of bacterial motility. *Mol Syst Biol*.
888 2007;3(1):128. doi:10.1038/msb4100166

889 41. Ebrahimi A, Schwartzman J, Cordero OX. Cooperation and spatial self-organization determine
890 rate and efficiency of particulate organic matter degradation in marine bacteria. *Proc Natl Acad*
891 *Sci USA*. 2019;116(46):23309-23316. doi:10.1073/pnas.1908512116

892 42. Drescher K, Nadell CD, Stone HA, Wingreen NS, Bassler BL. Solutions to the Public Goods
893 Dilemma in Bacterial Biofilms. *Current Biology*. 2014;24(1):50-55.

894 doi:10.1016/j.cub.2013.10.030

895 43. Alcolombri U, Peaudecerf FJ, Fernandez VI, Behrendt L, Lee KS, Stocker R. Sinking enhances
896 the degradation of organic particles by marine bacteria. *Nat Geosci*. 2021;14(10):775-780.
897 doi:10.1038/s41561-021-00817-x

898 44. Fenchel T. Microbial Behavior in a Heterogeneous World. *Science*. 2002;296(5570):1068-1071.
899 doi:10.1126/science.1070118

900 45. Preheim SP, Boucher Y, Wildschutte H, et al. Metapopulation structure of Vibrionaceae among
901 coastal marine invertebrates. *Environmental Microbiology*. 2011;13(1):265-275.
902 doi:10.1111/j.1462-2920.2010.02328.x

903 46. Yawata Y, Carrara F, Menolascina F, Stocker R. Constrained optimal foraging by marine
904 bacterioplankton on particulate organic matter. *Proc Natl Acad Sci USA*. 2020;117(41):25571-
905 25579. doi:10.1073/pnas.2012443117

906 47. McDougald D, Rice SA, Barraud N, Steinberg PD, Kjelleberg S. Should we stay or should we go:
907 mechanisms and ecological consequences for biofilm dispersal. *Nat Rev Microbiol*.
908 2012;10(1):39-50. doi:10.1038/nrmicro2695

909 48. Thomas F, Barbeyron T, Tonon T, Génicot S, Czjzek M, Michel G. Characterization of the first
910 alginolytic operons in a marine bacterium: from their emergence in marine Flavobacteriia to their
911 independent transfers to marine Proteobacteria and human gut Bacteroides: Emergence and
912 transfer of alginolytic operons. *Environmental Microbiology*. 2012;14(9):2379-2394.
913 doi:10.1111/j.1462-2920.2012.02751.x

914 49. Dudek M, Dieudonné A, Jouanneau D, et al. Regulation of alginate catabolism involves a GntR
915 family repressor in the marine flavobacterium Zobellia galactanivorans DsijT. *Nucleic Acids*
916 *Research*. 2020;48(14):7786-7800. doi:10.1093/nar/gkaa533

917 50. Chubukov V, Gerosa L, Kochanowski K, Sauer U. Coordination of microbial metabolism. *Nat*
918 *Rev Microbiol*. 2014;12(5):327-340. doi:10.1038/nrmicro3238

919 51. Martínez-Antonio A, Janga SC, Salgado H, Collado-Vides J. Internal-sensing machinery directs
920 the activity of the regulatory network in Escherichia coli. *Trends in Microbiology*. 2006;14(1):22-
921 27. doi:10.1016/j.tim.2005.11.002

922 52. Wall ME, Hlavacek WS, Savageau MA. Design of gene circuits: lessons from bacteria. *Nat Rev*
923 *Genet*. 2004;5(1):34-42. doi:10.1038/nrg1244

924 53. Bassler BL, Gibbons PJ, Yu C, Roseman S. Chitin utilization by marine bacteria. Chemotaxis to
925 chitin oligosaccharides by Vibrio furnissii. *Journal of Biological Chemistry*.
926 1991;266(36):24268-24275. doi:10.1016/S0021-9258(18)54224-1

927 54. Meibom KL, Li XB, Nielsen AT, Wu CY, Roseman S, Schoolnik GK. The *Vibrio cholerae* chitin
928 utilization program. *Proc Natl Acad Sci USA*. 2004;101(8):2524-2529.
929 doi:10.1073/pnas.0308707101

930 55. Keegstra JM, Carrara F, Stocker R. The ecological roles of bacterial chemotaxis. *Nat Rev*
931 *Microbiol*. 2022;20(8):491-504. doi:10.1038/s41579-022-00709-w

932 56. Clerc EE, Raina JB, Keegstra JM, et al. Strong chemotaxis by marine bacteria towards
933 polysaccharides is enhanced by the abundant organosulfur compound DMSP. *Nat Commun*.
934 2023;14(1):8080. doi:10.1038/s41467-023-43143-z

935 57. Konishi H, Hio M, Kobayashi M, Takase R, Hashimoto W. Bacterial chemotaxis towards
936 polysaccharide pectin by pectin-binding protein. *Sci Rep*. 2020;10(1):3977. doi:10.1038/s41598-

937 020-60274-1

938 58. Norris N, Alcolombri U, Keegstra JM, et al. Bacterial chemotaxis to saccharides is governed by a
939 trade-off between sensing and uptake. *Biophysical Journal*. 2022;121(11):2046-2059.
940 doi:10.1016/j.bpj.2022.05.003

941 59. Blackburn N, Fenchel T. Influence of bacteria, diffusion and shear on micro-scale nutrient
942 patches, and implications for bacterial chemotaxis. *Mar Ecol Prog Ser*. 1999;189:1-7.
943 doi:10.3354/meps189001

944 60. Blackburn N, Fenchel T, Mitchell J. Microscale Nutrient Patches in Planktonic Habitats Shown
945 by Chemotactic Bacteria. *Science*. 1998;282(5397):2254-2256.
946 doi:10.1126/science.282.5397.2254

947 61. Smriga S, Fernandez VI, Mitchell JG, Stocker R. Chemotaxis toward phytoplankton drives
948 organic matter partitioning among marine bacteria. *Proc Natl Acad Sci USA*. 2016;113(6):1576-
949 1581. doi:10.1073/pnas.1512307113

950 62. Ronce O. How Does It Feel to Be Like a Rolling Stone? Ten Questions About Dispersal
951 Evolution. *Annu Rev Ecol Evol Syst*. 2007;38(1):231-253.
952 doi:10.1146/annurev.ecolsys.38.091206.095611

953 63. Fenchel T. Motility of bacteria in sediments. *Aquat Microb Ecol*. 2008;51:23-30.
954 doi:10.3354/ame01182

955 64. Rumbaugh KP, Sauer K. Biofilm dispersion. *Nat Rev Microbiol*. 2020;18(10):571-586.
956 doi:10.1038/s41579-020-0385-0

957 65. Hehemann JH, Arevalo P, Datta MS, et al. Adaptive radiation by waves of gene transfer leads to
958 fine-scale resource partitioning in marine microbes. *Nat Commun*. 2016;7:12860.
959 doi:10.1038/ncomms12860

960 66. Tibbles BJ, Rawlings DE. Characterization of nitrogen-fixing bacteria from a temperate saltmarsh
961 lagoon, including isolates that produce ethane from acetylene. *Microb Ecol*. 1994;27(1).
962 doi:10.1007/BF00170115

963 67. D'Souza G, Waschina S, Pande S, Bohl K, Kaleta C, Kost C. Less is more: Selective advantages
964 can explain the prevalent loss of biosynthetic genes in bacteria. *Evolution*. 2014;68(9):2559-2570.
965 doi:10.1111/evo.12468

966 68. Mathis R, Ackermann M. Response of single bacterial cells to stress gives rise to complex history
967 dependence at the population level. *Proc Natl Acad Sci USA*. 2016;113(15):4224-4229.
968 doi:10.1073/pnas.1511509113

969 69. Brettin T, Davis JJ, Disz T, et al. RASTtk: A modular and extensible implementation of the
970 RAST algorithm for building custom annotation pipelines and annotating batches of genomes. *Sci*
971 *Rep*. 2015;5(1):8365. doi:10.1038/srep08365

972 70. Kanehisa M, Sato Y, Morishima K. BlastKOALA and GhostKOALA: KEGG Tools for
973 Functional Characterization of Genome and Metagenome Sequences. *Journal of Molecular*
974 *Biology*. 2016;428(4):726-731. doi:10.1016/j.jmb.2015.11.006

975 71. Cheng D, Jiang C, Xu J, Liu Z, Mao X. Characteristics and applications of alginate lyases: A
976 review. *International Journal of Biological Macromolecules*. 2020;164:1304-1320.
977 doi:10.1016/j.ijbiomac.2020.07.199

978 72. Zhang H, Yohe T, Huang L, et al. dbCAN2: a meta server for automated carbohydrate-active
979 enzyme annotation. *Nucleic Acids Res*. 2018;46(W1):W95-W101. doi:10.1093/nar/gky418

980 73. NCBI Resource Coordinators. Database resources of the National Center for Biotechnology
981 Information. *Nucleic Acids Res*. 2016;44(Database issue):D7-D19. doi:10.1093/nar/gkv1290

982 74. Altschul SF, Gish W, Miller W, Myers EW, Lipman DJ. Basic local alignment search tool. *J Mol*
983 *Biol*. 1990;215(3):403-410. doi:10.1016/S0022-2836(05)80360-2

984 75. Almagro Armenteros JJ, Tsirigos KD, Sønderby CK, et al. SignalP 5.0 improves signal peptide
985 predictions using deep neural networks. *Nat Biotechnol*. 2019;37(4):420-423.
986 doi:10.1038/s41587-019-0036-z

987 76. Juncker AS, Willenbrock H, von Heijne G, Brunak S, Nielsen H, Krogh A. Prediction of
988 lipoprotein signal peptides in Gram-negative bacteria. *Protein Sci*. 2003;12(8):1652-1662.

989 77. Andrews S. FastQC: A Quality Control Tool for High Throughput Sequence Data [Online].
990 Available online at: http://www.bioinformatics.babraham.ac.uk/projects/fastqc/. Published online
991 2010. http://www.bioinformatics.babraham.ac.uk/projects/fastqc/

992 78. Bolger AM, Lohse M, Usadel B. Trimmomatic: a flexible trimmer for Illumina sequence data.
993 *Bioinformatics*. 2014;30(15):2114-2120. doi:10.1093/bioinformatics/btu170

994 79. Langmead B, Salzberg SL. Fast gapped-read alignment with Bowtie 2. *Nat Methods*.
995 2012;9(4):357-359. doi:10.1038/nmeth.1923

996 80. Danecek P, Bonfield JK, Liddle J, et al. Twelve years of SAMtools and BCFtools. *Gigascience*.
997 2021;10(2):giab008. doi:10.1093/gigascience/giab008

998 81. Liao Y, Smyth GK, Shi W. featureCounts: an efficient general purpose program for assigning
999 sequence reads to genomic features. *Bioinformatics*. 2014;30(7):923-930.
1000 doi:10.1093/bioinformatics/btt656

1001 82. Love MI, Huber W, Anders S. Moderated estimation of fold change and dispersion for RNA-seq
1002 data with DESeq2. *Genome Biology*. 2014;15(12):550. doi:10.1186/s13059-014-0550-8

1003 83. Benjamini Y, Hochberg Y. Controlling the False Discovery Rate: A Practical and Powerful
1004 Approach to Multiple Testing. *Journal of the Royal Statistical Society: Series B*
1005 *(Methodological)*. 1995;57(1):289-300. doi:10.1111/j.2517-6161.1995.tb02031.x

1006 84. Luo W, Brouwer C. Pathview: an R/Bioconductor package for pathway-based data integration
1007 and visualization. *Bioinformatics*. 2013;29(14):1830-1831. doi:10.1093/bioinformatics/btt285

1008 85. Midani FS, Collins J, Britton RA. AMiGA: Software for Automated Analysis of Microbial
1009 Growth Assays. Silva-Rocha R, ed. *mSystems*. 2021;6(4):e00508-21.
1010 doi:10.1128/mSystems.00508-21